Spaceborne Inferences of Cloud Microstructure and Precipitation Processes: Synthesis, Insights and Implications

A Paper from the Symposium on Cloud Systems, Hurricanes and TRMM: Celebration of Dr. Joanne Simpson's Career --- the First 50 Years

By

Daniel Rosenfeld
Hebrew University of Jerusalem
Jerusalem, Israel

And

William L. Woodley
Woodley Weather Consultants
Littleton, Colorado

March 28, 2001

Abstract

Spaceborne inferences of cloud microstructure and precipitation-forming processes with height have been used to investigate the effect of ingested aerosols on clouds and to integrate the findings with past cloud physics research. The inferences were made with a method that analyzes data from NOAA/AVHRR and TRMM/VIRS sensors to determine the effective radius of cloud particles with height. In addition, the TRMM/PR made it possible to measure the rainfall simultaneously with the microphysical retrievals, which were validated by aircraft cloud physics measurements under a wide range of conditions. For example, the satellite inferences suggest that vigorous convective clouds over many portions of the globe remain supercooled to near

–38^{o}C, the point of homogeneous nucleation. These inferences were then validated in Texas and Argentina by in-situ measurements using a cloud physics jet aircraft.

This unique satellite vantage point has documented enormous variability of cloud conditions in space and time and the strong susceptibility of cloud microstructure and precipitation to the ingested aerosols. This is in agreement with past cloud physics research. In particular, it has been documented that smoke and air pollution can suppress both water and ice precipitation-forming processes over large areas. Measurements in Thai convective clouds suggest that the suppression of coalescence can decrease areal rainfall by as much as a factor of two. It would appear, therefore, that pollution has the potential to alter the global climate by suppressing rainfall and decreasing the net latent heating to the atmosphere and/or forcing its redistribution. In addition, it appears that intense lightning activity, as documented by the TRMM LIS sensor, is usually associated with microphysically highly "continental" clouds having large concentrations of ingested aerosols, great cloud-base concentrations of tiny droplets, and high cloud-water contents. Conversely, strongly "maritime" clouds, having intense coalescence, early fallout of the hydrometeors and glaciation at warm temperatures, show little lightning activity. By extension these results suggest that pollution can enhance lightning activity.

The satellite inferences suggest that the effect of pollution on clouds is greater and on a much larger scale than any that have been documented for deliberate cloud seeding. They also provide insights for cloud seeding programs. Having documented the great variability in space and time of cloud structure, it is likely that the results of many cloud seeding efforts have been mixed and inconclusive, because both suitable and unsuitable clouds have been seeded and grouped together for evaluation. This can be addressed in the future by partitioning the cases based on the microphysical structure of the cloud field at seeding and then looking for seeding effects within each partition.

This study is built on the scientific foundation laid by many past investigators and its results can be viewed as a synthesis of the new satellite methodology with their findings. Especially noteworthy in this regard is Dr. Joanne Simpson, who has spent much of her career studying and modeling cumulus clouds and specifying their crucial

role in driving the hurricane and the global atmospheric circulation. She also was a pioneer in early cloud seeding research in which she emphasized cloud dynamics rather than just microphysics in her seeding hypotheses and in her development and use of numerical models. It is appropriate, therefore, that we offer this paper to acknowledge Dr. Joanne Simpson and her many colleagues who paved the way for our research effort.

1.0 Introduction

This study builds on past research and incorporates new technology, findings and insights to develop a cloud physics synthesis concerning the effect of ingested aerosols on clouds. The results are presented in the context of the 50-year career of Dr. Joanne Simpson during which our meteorological discipline has come full circle. It started with imperfect cloud models and inadequate cloud physics observations, much of it in the context of cloud seeding research efforts. It then moved to space where space technology provided results and insights that had never been possible before. Now we are back where we started but with greatly improved technology, observations, and insights that benefit cloud seeding programs and make it possible to address the effect of pollution and natural aerosols on rainfall and on the global climate system.

The current interest has been on the role that high concentrations of tiny cloud condensation nuclei (CCN) play in generating highly reflective clouds by altering the cloud drop size distribution. Such clouds return a greater percentage of incoming radiation to space than they would have had they not ingested the high concentrations of small CCN. This CCN "pollution" is postulated as a possible cooling mechanism that might act to offset the global warming due to increased concentrations of carbon dioxide (CO_2). This is now called the Twomey effect (Twomey et al., 1987).

As shown herein, anthropogenic pollution also enters into the global equation. Smoke from biomass burning and from industry and urban pollution acts to suppress coalescence and ice processes in cloud. This has the potential to decrease and/or redistribute the precipitation and the global heating due to the precipitation. Thus, the

effect of anthropogenic aerosols does not stop at radiative processes; they can also have a profound detrimental impact on precipitation. These insights would not have been possible without the new spaceborne measurements to be discussed here.

The opportunity to present new research results in a paper honoring the long and illustrious career of Dr. Joanne Simpson is a once-in-a-lifetime opportunity. We hope that we will be judged to have made the most of it. Joanne's career has been a long and fascinating journey for all who have had the pleasure and honor to travel it with her. This is recounted in this paper in the context of the research performed by its two authors, who owe much to Joanne for her help and inspiration. It begins with cloud seeding concepts and studies and this is followed by new research results, which document the apparent role of aerosols and coalescence in the production of rain from clouds.

2.0 Cloud Seeding Concepts and Studies

Convective clouds figured prominently in the development and testing of a conceptual model for the reduction of hurricane wind speeds through glaciogenic seeding of deep convection in bands exterior to the hurricane eyewall. As Director of Project Stormfury, Dr. Joanne Simpson worked on this intriguing problem with her husband Bob and a cadre of other scientists. The key initial point in the conceptual model was the assumption that deep convective clouds in the hurricane remain supercooled through a considerable depth of the troposphere, making them suitable for glaciogenic seeding. Microphysical measurements later revealed, however, that these conditions are not met in the hurricane. On the contrary, deep convection in the hurricane glaciates typically at temperatures > -10^{o}C. Had this been known in advance, the Stormfury program might never have begun. This finding emphasizes the importance of cloud microphysical measurements.

Scientific spin-offs from Project Stormfury under Joanne Simpson soon proved to be more important than Stormfury itself. Joanne pursued development of her one-dimensional cloud model (Witt and Malkus, 1959) in conjunction with randomized

experimentation on supercooled convective clouds over the Caribbean and then in Florida. In a classic paper (Simpson et al., 1967) Joanne used her simple model to predict the growth response (called "seedability") of treated clouds and compared her predictions to what was observed following seeding (seeding effect). There was excellent agreement between the predicted and observed growths of the unseeded and seeded clouds, respectively. This paper validated Joanne's view that one of the best ways to understand clouds is to perturb their natural state through cloud seeding. It also gave scientific credibility to cloud seeding.

This separation of seeded and non-seeded clouds into two distinct populations based on model predictions was a very persuasive finding for the postulate that seeding with a glaciogenic agent could affect the dynamics of clouds through the heat released during glaciation. This model became known as the "dynamic seeding" conceptual model. Dr. Woodley worked initially with Joanne on its development and testing until she left for other scientific challenges at the University of Virginia and then NASA. He continued his study of the effect of cloud seeding on cloud structure and precipitation and was joined by Dr. Rosenfeld in 1980. They continue their collaboration to this day.

The development of cloud seeding concepts has been hindered by dynamical and microphysical uncertainties. The initial dynamic seeding conceptual model conceded that the seeding might make the seeded volume less precipitation efficient because of the expected high concentration of ice particles following seeding. It was assumed, however, that the presumed microphysical inefficiencies of converting cloud water into precipitation would be overwhelmed by increases in cloud size, duration and rainfall. Although such changes have been observed following seeding (Simpson et al, 1967; Simpson and Woodley, 1971), they provide no information regarding the efficiency of the cloud microphysical processes.

A second uncertainty with respect to cloud seeding experiments is how an effect of seeding in one cloud might be communicated to other nearby clouds. Joanne (Simpson, 1980) argued persuasively that enhancement of downdrafts by seeding is the

mechanism whereby an effect of seeding is communicated to other clouds. The downdrafts are postulated to result in regions of convergence between the downdraft outflows and the ambient flows or with outflows from other clouds. New clouds then grow in the convergent regions, resulting in the broadening and deepening of the precipitation area.

These ideas were incorporated into the dynamic seeding conceptual model (Woodley et al, 1982), which was revised further as of 1993 (Rosenfeld and Woodley, 1993). By this time, the conceptual model had come full circle from its original version to postulate that seeding makes clouds more microphysically efficient by producing graupel, which grows preferentially at the expense of the cloud water. It is obvious that any model that purports to explain natural cloud processes and their alteration by seeding must address these interactive dynamical and microphysical processes.

3.0 The Role of Aerosols and Coalescence in Rain Production

The cloud seeding conceptual model as developed by the authors (Rosenfeld and Woodley, 1993) predicts that the effect of seeding will be a function in part of the aerosols ingested by clouds and by their ability to develop raindrops through coalescence. This explains the keen interest of the authors in coalescence processes. They are of great importance to TRMM as well, because coalescence leads to rainfall, leaving the heat of condensation irreversibly to the atmosphere. Such irreversible heat releases are characteristically larger in microphysically-maritime clouds than in clouds of continental character, because they precipitate a larger fraction of their cloud water.

The fundamental difference between microphysically continental and maritime clouds is the drop size distribution near their bases. Clouds are considered quite maritime when the cloud-base droplet concentration is less than 100 droplets cm^{-3}, whereas continental clouds have cloud-base droplet concentrations greater by about an order of magnitude. The terms “continental” and “maritime” originate from the observation that the drop-size distribution near cloud base is governed by the distribution of the cloud

condensation nuclei (CCN), continents being the source of high CCN concentrations and marine environments being the source of low CCN concentrations. It was recognized more than 40 years ago that continental clouds have larger "colloidal stability" than maritime clouds (Squires, 1958). Laboratory experiments of relevance to coalescence in clouds in CCN rich and lean environments (Gunn and Phillips, 1957), led to the suggestion that highly continental clouds, which form in a CCN rich atmosphere, would produce less precipitation. It has been widely accepted since then that, in the absence of ice processes, microphysically continental clouds are less precipitation efficient and produce less rainfall than "clean" maritime clouds of the same size, because coalescence processes are weaker in continental clouds, resulting in a slower conversion of their water into precipitation.

These differences between continental and maritime clouds were the basis for the early hygroscopic seeding conceptual models aimed at augmenting precipitation by enhancing coalescence processes (Bowen, 1952; Biswas and Dennis, 1971; Cotton, 1982). Braham (1964) has postulated that enhancement of coalescence in supercooled clouds can enhance the ice precipitation processes. The larger drops freeze faster and at warmer temperatures (Bigg, 1953), and grow faster by riming than drops of comparable mass would have grown by coalescence (Johnson, 1987; Pinsky et al., 1998). This likely explains the presence of so much ice in deep convection in the hurricane. The hygroscopic seeding conceptual model of recent experiments has been amended to include the positive impact of enhanced coalescence on mixed phase precipitation processes (Mather et al., 1997; Cooper et al., 1997).

Modeling studies (Reisin et al., 1996) of the rainfall amounts from clouds with top temperatures of about -20^{o}C provided some quantitative assessment of the importance of coalescence to the production of rainfall from clouds. A simulated change of the CCN concentrations at 1% supersaturation from maritime (100 cm^{-3}) to continental (1100 cm^{-3}), resulted in an 86% decrease in the simulated rainfall.

The importance of coalescence in the production of rainfall from Thai convective cells has been investigated by Rosenfeld and Woodley using volume-scan radar observations from the AARRP (Applied Atmospheric Research Resources Project) 10-cm, Doppler radar in northwest Thailand. The radar estimates of cell properties were partitioned using in-situ observations of the presence or absence of detectable raindrops on the windshield of the project Aero Commander seeder aircraft as it penetrated the updrafts of growing convective towers, 200 - 600 m below their tops at about the -8^{o}C level (about 6.5 km MSL). Cells observed to contain detectable raindrops during these aircraft penetrations were found to have smaller first-echo depths than cells without observed raindrops when growing through the aircraft penetration level, where first-echo depth is the difference between first-echo height and the height of cloud base. Although cloud dynamics likely played a role, this faster formation of raindrops is thought to be due primarily to a rapid onset of coalescence in the convective cells.

Rain volumes produced by the aircraft measured rain clouds were estimated, using 5-minute sequences of S-Band radar-volume scans. Each rain cell was represented by a reflectivity maximum, bounded at the 12-dBZ level or the line of minimum between it and a neighboring cell. The rain volumes were determined by time-area integration of the rain intensities of the tracked rain cells, using the methodology of long-tracked cells as described by Rosenfeld and Woodley (1993). Convective cells exhibiting a rapid onset of coalescence (Category 2 clouds with detectable raindrops when growing through the aircraft penetration level) produced over a factor of two more rainfall than comparably sized cells in which the onset of coalescence was slower (Category 1 clouds with no detectable raindrops when growing through the aircraft penetration level). This was true also for convective cloud systems over an area covering 1,964 km^2 (Table 1). Both ratios have impressive rerandomization (permutation) statistical P values, defining the probability that the result was obtained by chance. In making the radar-rainfall estimates, the rain intensities (R) were calculated from the reflectivity (Z) by using the Z-R relationship $Z = 300R^{1.5}$ on the 2-km altitude (cloud base) reflectivities. A systematic bias in the Z-R relation for clouds with active warm rainfall and other clouds would also induce a systematic difference in the radar inferred rain volume. However, warm rain

produces typically smaller reflectivitues for the same rain intensity than clouds with mixed phase precipitation processes. This observation underlies the selection of Z-R relationships for the WSR-88D radar network, using for "summer deep convection" the relation $Z=300R^{1.4}$ (Woodley and Herndon, 1970), and using for "Tropical convective systems" the relation $Z=250R^{1.2}$ (Rosenfeld et al., 1993). According to this, if there is any bias due to differences in the Z-R relations, it would work to underestimate the differences under the assumption of fixed Z-R relations.

Table 1

Radar-Estimated Rain Volumes ($m^3 \times 10^3$) for Convective Cells and Convective Cloud Systems as a Function of Coalescence Category
(The statistical P values for the ratios were obtained from rerandomization procedures)

Convective Type	Category 2	Category 1	Category 2/ Category 1	Rerandomization P-Value
Convective Cells	267.9	130.6	2.05	0.016
Convective Cloud Systems	6204.4	2631.8	2.36	0.000

It was found also that the rain production of convective cells increases with maximum echo top height in both coalescence categories, but the increase is greater for clouds exhibiting a rapid onset of coalescence as shown in Fig. 1. The data are plotted at the center point of 2 km intervals of maximum echo-top height.

The mean rain-volume differences (dashed line) and ratios of mean rain volumes (solid curve) versus maximum precipitation echo top height for cells growing on days with weak coalescence activity (Category 1) and on days with strong coalescence activity

(Category 2) are shown in Fig. 2. Although the ratios of the rain volume between convective cells exhibiting a rapid onset of coalescence and those with slower coalescence activity are impressively high for the shallow convective cells, in which condensation-coalescence is the dominant precipitation mechanism, the volumetric rain differences are rather small.

On the other hand, for the deep convective cells, in which mixed-phase precipitation development processes are dominant, the rain-volume ratios are lower but still physically significant; and they are associated with volumetric rain differences that are important to the overall rainfall of the area. For example, deep tropical cumulonimbus cells (all cells with Hmax > 10 km) that exhibit a rapid onset of coalescence produce about a factor of two more rain volume than cells with slower coalescence activity. This finding has high statistical significance (see Table 1). The volumetric rainfall difference is 253 x 10^3 m^3 per cell with a P-value smaller than 0.03 from a "t" test, assuming unequal variances. Most important, lifecycle analysis of convective cloud systems in which the convective cells reside showed that the results for the cell scale are preserved on the scale of cloud systems (Table 1).

These findings highlight the important role that coalescence plays in the production of rain from both shallow and deep convective cells and cloud systems and they provide valuable insights into natural cloud processes. Other meteorological factors (e.g., cloud dynamics) being equal, they also help in understanding regional differences in rainfall and their probable causes through the linkages between cloud condensation nuclei (CCN), cloud droplet size distribution, coalescence and rainfall amounts. These results suggest also that pollution, containing high concentrations of CCN that suppress coalescence, is likely to act detrimentally on rain forming processes in clouds. If the pollution is extensive, it has the potential to affect the global climate. The effects of seeding should also be different in polluted clouds and non-polluted clouds.

4.0 The Role of Satellites in Cloud and Precipitation Physics

4.1 Overview

The microstructure of clouds and precipitation is typically determined by flying an instrumented cloud physics aircraft into the clouds for in situ measurements, although the NCAR Electra Doppler Radar (ELDORA) and the NASA's ER2-Doppler radar (EDOP) on aircraft have been used for remote sensing of cloud properties. This permits only limited measurements in space and time. Increasingly, however, the internal properties of clouds have been inferred remotely using either radar or satellite. This has allowed much greater time and space sampling. The combined use of all systems is the best of all worlds. The instrumented aircraft still provides the measurement standard while radar and satellites allow for a much-expanded view.

Recent breakthroughs in the use of satellites to infer cloud microphysical properties have been especially noteworthy. Traditionally, the single visible and single IR channels on most satellites provided only very limited information about the cloud properties, such as visible reflectance, cloud top temperature, and a crude estimate of vertically integrated cloud water. Additional channels on NOAA/AVHRR and TRMM/VIRS in the solar IR (1.6 μm), mid-IR (3.8 μm) and far IR (10.8 and 12.0 μm), and many more on recently launched MODIS onboard of TERRA, now make it possible to obtain additional information about a wide range of cloud properties. Among them are cloud thickness and cloud composition, i.e., effective radius of cloud top particles, and whether they are composed of water or ice.

The added multispectral information makes it possible to retrieve various properties of various types of clouds and surfaces. This can be used for classification of

clouds into physically meaningful types. It can be also used to identify the clouds even over a background of ice and snow, or lower cloud layers. The clouds can be classified according to their composition: water, supercooled water, mixed-phase or ice clouds of various types. The evolution of the cloud composition and particle size in the vertical can be used most of the time to infer the precipitation properties: non-precipitating, drizzle, warm rain, mixed-phase or ice precipitation processes.

The possibility of obtaining such information from multispectral analyses of satellite data opens a whole new range of potential applications, some of which were not contemplated only a few years ago. Although the potential for detection of supercooled water and icing conditions was already recognized (Schickel et al., 1994), other applications related to precipitation are just starting to emerge.

A particularly intriguing prospect is the possibility of detecting how cloud composition and precipitation are affected by natural (e.g., desert dust) and anthropogenic aerosols (e.g., smoke from burning vegetation, urban and industrial air pollution). Many of these potential products and new directions of research are currently in their early developmental stages. These new possibilities represent yet untapped potential from geostationary and orbiting satellites with multispectral capabilities that have been launched during recent years.

4.2 Physical basis of the satellite methodology

The family of sensors on board the recent satellites has a family of spectral bands in the solar and terrestrial portion of the radiation spectrum. This is illustrated in Fig. 3 for the Meteosat Second Generation (MSG) satellite, which has 12 spectral bands. The situation for the GOES, NOAA/AVHRR and TRMM/VIRS is similar, but with some of the channels missing. These channels make it possible to measure additional parameters in addition to visible reflectance and the thermal emission temperature.

The fundamental reason for the added capabilities is the differences in the interaction of the radiation with cloud particles at different wavelengths. A very important contribution of the added multispectral capability comes from the dependence of the absorption of water and ice on the wavelength, as illustrated in Fig. 4. The absorption of the solar radiation by the cloud particles occurs within their volume (αr^3), whereas the scattering of the radiation occurs at their surface (αr^2). The absorption detracts from the overall back-scattered radiation. This results in net reflected radiation to the satellite αr^{-1}. Therefore, the reflected solar radiation in absorbing wavelengths is inversely proportional to the particle size. Taking into account the relative angles of the sun, object and sensor, it is possible to retrieve the effective radius of cloud particles, r_e. The effective radius is proportional to the sum of the volumes divided by the sum of the surface areas of the particles in the measurement volume of the satellite pixel. The large absorption in the 1.6 and 3.8 μm bands makes it possible to use these channels for retrieving r_e, in contrast to the non-absorbing visible channel (Arking and Childs, 1985; Nakajima and King, 1990).

In reality, the calculations of the effective radius need to take into account effects such as multiple scattering within the clouds, correction for absorption by gases, upwelling radiation from the surface through the clouds, possible multiple layer clouds, and shadowing effects. Most of these errors increase with increasing solar zenith angles, limiting reasonably accurate retrievals only to times where the sun is more than about 20^o above the horizon, and satellite zenith angle < ~50^o.

Retrieval of r_e has been applied extensively to marine stratocumulus, in order to measure the impact of aerosols on cloud microstructure and through that on earth radiation budget. Attention was directed to this subject shortly after launch of the first NOAA orbiting satellites with the Advanced Very High Resolution Radiometer (AVHRR), revealing ship tracks consisting of polluted clouds with enhanced albedo and reduced droplet sizes (Coakley et al., 1987). An example of ship tracks in the north Pacific in shown in Fig. 5.

The pollution particles emitted from the ship stacks act as CCN, redistributing the fixed amount of cloud water that must condense into a larger number of smaller droplets (Radke et al., 1989). It was recognized then that the reduced droplet size suppressed the

coalescence and drizzle, thus preventing loss of cloud water. The effects of larger amounts of cloud water in smaller droplets are to increase the cloud reflectance of solar radiation. Similar effects were observed over land, where the impact of smoke on shallow tropical convective clouds was shown to decrease the droplets effective radius from about 15 microns to 9 microns (Kaufman and Fraser, 1997). The increased reflectance, mainly in the solar infra red, has been considered as a cooling mechanism partially counteracting global warming due to the increased greenhouse gases (Houghton et al., 1994). However, the potential applications of 1.6 μm and 3.8 μm reflectance go much beyond the important subject of cloud-aerosol impacts on the earth's radiative budget. The reported (Kaufman and Fraser, 1997) reduction of cloud droplets below the threshold of 14-microns, which is the minimum required size for effective coalescence (Rosenfeld and Gutman, 1994), means that in addition to the radiative effects, the smoke also had a suppressive effect on precipitation. In the next sections we will see how the multispectral observations can provide us with qualitative (Section 4.4) and quantitative (Section 4.5) information about cloud microstructure and precipitation.

4.3 Multispectrally-based cloud classification

The various channels provide different kinds of information. Whereas the interpretation of the visible and thermal infra red window channels is well known, the information content of the near infra red (NIR, 1.6 and 3.8 μm) reflectance deserves more attention. For clouds composed of very small water droplets, the scattering dominates the absorption, and therefore the ratio of NIR/visible reflectance will be closest to unity. For increasingly large droplets the NIR reflectance decreases and the ratio decreases. Because ice absorbs more strongly than water at 3.8 μm, and even more so at 1.6 μm (See Fig. 4), the reflectance in these channels is even smaller for ice particles. Therefore, ratios of NIR/visible reflectance approaching zero indicate ice surfaces or clouds. Therefore, the combination of the visible and NIR reflectance provide valuable information about the cloud optical thickness and composition. With the added temperature information from the thermal infra red window, a highly detailed cloud classification and characterization can be made. Rendering the three parameters in red-green-blue color composite is natural for human perception, creating colors

that correspond to the different cloud types, as described in Table 2 (Rosenfeld and Lensky, 1998).

This qualitative classification can be readily used for a large number of applications, including:

Detection of aircraft icing conditions: icing occurs when aircraft fly in supercooled water clouds. Such clouds should be detectable under most conditions according to Table 2.

Detection of fog or low clouds on the background of a snow-covered surface: Water clouds and snow or ice surfaces are very different according to Table 2. The frozen surface appears purple, and the water clouds appear white or yellow on the purple background.

Distinction between precipitating and non-precipitating clouds: Precipitation forming processes require that a cloud must be deep (highly reflective in the visible) and composed of large droplets or ice particles (small reflectance at 3.8 μm). This can be identified by the appropriate entries in Table 2.

Identification of air pollution: Low level clouds composed of small droplets (large reflectance at 3.8 μm) are indicative of an air mass containing a large concentration of aerosols. The polluted clouds appear as relatively bright patches or stripes on the pink background of clouds with large droplets in clean air. The classical example for that is ship tracks, as they appear in Fig. 5. Such pollution tracks have been identified also in clouds over land areas (Rosenfeld, 2000).

4.4 Quantitative multispectral methods.

While human perception more readily absorbs large quantities of qualitative information, especially when presented with the appropriate method of visualization,

greater benefits and deeper insights can come from quantitative analyses using computerized algorithms. Some of the methods and the added insights gained by them are presented in this section.

Some of the more important parameters that can be derived for each satellite pixel from the multispectral satellite data in daylight conditions are:

- Cloud reflectance in the visible (R), normalized for the solar zenith angle. For Lambertian cloud surfaces (rarely actually realized) the reflectance equals the albedo. Under some assumptions, optical depth and liquid water path can be retrieved from the visible reflectance.

- Cloud top temperature (T). This can be obtained from the thermal channel at 10.8 μm, and can be made more accurate with a correction for water vapor, when using the 12.0 μm and water vapor channels.

- Cloud particle effective radius, r_e. Using the 1.6 and 3.8 um reflectance, it is possible to calculate the r_e of a cloud top. The calculation is based on the assumption that the cloud is composed of water drops, the cloud completely fills the pixel, and the cloud is thick, i.e., a negligible amount of radiation from the surface at 1.6 or 3.8 μm is upwelling through the cloud top. If this is not the case the surface reflectance must be known precisely (Arking and Childs, 1985).
- Cloud microphysical phase: water, mixed phase or ice. Clouds with $T>0^oC$ must be water clouds. However, only clouds at $T\leq -39^oC$ can be determined unambiguously as ice on the single pixel level, because supercooled water clouds can exist down to -38^oC (Rosenfeld and Woodley, 2000).

Much more information about the cloud microstructure and precipitation forming processes in convective clouds can be obtained from analyses of complete cloud clusters, residing in areas containing thousands of satellite pixels. The underlying assumption is that the microphysical evolution of a convective cloud can be represented by composition

of the instantaneous values of the tops of convective clouds at different heights. This is based on the knowledge that cloud droplets form mainly at the base of convective clouds, and grow with increasing height or decreasing T. The form of dependence of r_e on T contains vital information about the cloud and precipitation processes, as described below. The T-r_e relations are obtained from an ensemble of clouds having tops covering a large range of T. Usually many pairs of T-r_e for each 1^oC interval are observed in a region containing a convective cloud cluster. The points with smaller r_e for a given T are typically associated with the younger cloud elements, whereas the larger r_e for the same T are associated with the more mature cloud elements, in which the droplets growth had more time to progress by coalescence, and ice particles had more time to develop. Therefore, it is useful to plot not only the median value of T-r_e relation, but also, say, the 15^{th} and 85^{th} percentiles (see Fig, 6), for representing the younger and more mature cloud elements within the measurement region.

Based on the shapes of the T-r_e relations, Rosenfeld and Lensky (1998) defined the following five microphysical zones in convective clouds:

1) *Diffusional droplet growth zone*: Very slow growth of cloud droplets with depth above cloud base, indicated by small $-dr_e/dT$.
2) *Droplet coalescence growth zone*: Large increase of the droplet growth with height, as depicted by large $-dr_e/dT$ at T warmer than freezing temperatures, indicating rapid cloud-droplet growth with depth above cloud base. Such rapid growth can occur there only by drop coalescence.
3) *Rainout zone*: A zone where r_e remains stable between 20 and 25 μm, probably determined by the maximum drop size that can be sustained by rising air near cloud top, where the larger drops are precipitated to lower elevations and may eventually fall as rain from the cloud base. This zone is so named, because droplet growth by coalescence is balanced by precipitation of the largest drops from cloud top. Therefore, the clouds seem to be raining out much of their water while growing. The radius of the drops that actually rain out from cloud tops is much

larger than the indicated r_e of 20-25 μm, being at the upper end of the drop size distribution there.

4) *Mixed phase zone*: A zone of large indicated droplet growth with height, occurring at $T<0^oC$, due to coalescence as well as to mixed phase precipitation formation processes. Therefore, the mixed phase and the coalescence zones are ambiguous at $0<T<-39^oC$. The conditions for determining the mixed phase zone within this range are specified in Rosenfeld and Lensky (1998).

5) *Glaciated zone*: A nearly stable zone of r_e having a value greater than that of the rainout zone or the mixed phase zone at $T<0^oC$.

These zones are idealizations. Not all clouds conform to this idealized picture. The transition between the coalescence and mixed phase zones, which are not separated by a rainout zone, cannot be determined, and are therefore set arbitrarily to -6^oC in accordance with aircraft observations. The height of the glaciation zone can be overestimated in the cases of highly maritime clouds that grow through a deep rainout zone, because the scarcity of water in the supercooled portions of the clouds causes small ice particles, which sometimes can be mistaken for a mixed phase cloud. Addition of more spectral bands can help in separating the water from the ice, irrespective of the particle size. On the other hand, in vigorous clouds with active coalescence the height of the glaciation zone can be underestimated, because the high amounts of large ice hydrometeors dominate the radiative properties of the clouds, even when they co-exist with cloud supercooled water.

All these microphysical zones are defined only for convective cloud elements. Multi-layer clouds start with small r_e at the base of each cloud layer. This can be used for distinguishing stratified from convective clouds by their microstructure. Typically, a convective cloud has a larger r_e than a layer cloud at the same height, because the convective cloud is deeper and contains more water in the form of larger drops.

In addition to the microphysical zones, it also can be determined that convective clouds start precipitating at $r_e > 14$ μm (Rosenfeld and Gutman, 1994; Gerber, 1996).

This can be used quantitatively for improving the accuracy of rainfall measurements from space, as demonstrated by Lensky and Rosenfeld (1997) for the NOAA/AVHRR.

Examples of the various microphysical zones have been obtained in clouds around the world. A simple case, showing the onset of glaciation, is the wave clouds shown in fig. 7. The small scatter of the effective radius for any given T and the repetitive behavior of each of the clouds, showing the jump of re at T=-32^{o}C, make a compelling case for inference of the glaciation temperature at this T.

Shallow convective clouds provide another simple example. Of interest here are clouds growing in a smoky atmosphere over the Amazon on 13 September 1998. The smoke aerosols are documented by the global plots of the Earth Probe TOMS Aerosol Index on this day (Fig. 8), showing pollution over the Amazon in the region of the growing clouds pictured in the processed TRMM image at 19:15 GMT (Fig. 9a). The 230-km swath of the precipitation radar is bounded by the white lines. The white stippling shows the radar echoes superimposed on the clouds that have been colorized according to the scheme in Table 2. The yellow crosses represent lightning flashes as detected by the TRMM/LIS, seen at the bottom of Figure 9a just outside the PR swath.

The T-r_e plot for area 1 in Fig. 9a is shown in Fig. 9b. The 15th, 50th and 85th percentiles for r_e vs. T for the area shown are plotted. These plots can e thought of as typifying the clouds in the area. Note that the clouds have a deep zone of diffusional droplet growth overlain by a shallower zone (0^{o}C to –10^{o}C) of droplet growth dominated by coalescence. The mixed-phase zone begins near –10^{o}C and continues to cloud top near –13^{o}C. Note the 14-micron precipitation threshold is not reached until –10^{o}C.

The vertical cross section for this case along the line in Fig. 9a is provided in Fig. 9c. Note that clouds with tops < 6.5 km do not produce precipitation and in the two that exceed that height precipitation is quite weak. Considering the location of the clouds over the tropical Amazon, this means strong suppression of coalescence and ice precipitation forming processes.

The next look is at a TRMM image of deep convective clouds growing in smoke over the Amazon two days later (Fig. 10a). The presentation is similar to that of Fig. 9a. These clouds have an even deeper zone of diffusional droplet growth overlain by a deep zone of mixed-phase processes (Fig. 10b). Glaciation is not indicated until –27^{o}C. The cross section along the line in Fig. 10a is quite different from that for the shallower clouds. The reflectivity profiles are strong from virtually cloud base to top, indicating that ice processes had produced large, highly-reflective ice particles in these clouds. Note that lightning activity (yellow crosses) is greater in this image than in Figure 9a.

In contrast to the clouds studied on 13 and 15 September 1998 are those growing in clean air over the Amazon on 13 April 1998 (Fig. 11a). These clouds obviously are quite maritime in character with deep zones of coalescence and rainout overlain by a shallow mixed-phase zone with a deep glaciated zone above that (Fig. 11b). Complete glaciation is indicated at –7^{o}C.

The vertical radar cross section (Fig 11c) show maximum reflectivities below 5 km and a greater distance between the visible cloud tops and their radar-measured tops than was the case for the deep continental clouds. Even very shallow clouds precipitate in agreement with the T-r_e plot (Fig. 11b) that shows virtually the entire cloud depth having droplets that exceed the 14-micron precipitation threshold. Such clouds convert their water into precipitation very fast and efficiently, in contrast to the clouds in the polluted air (Figs 9 and 10).

In order to make the point that these clouds are highly maritime, even though they are more than 1000 km away from the closest ocean, a comparison with truly equatorial oceanic clouds is made, in the form of a TRMM image of deep cumulus and cumulonimbus clouds over the equatorial Pacific near Kwajalein at 02:51 GMT on 5 November 1998 (Fig. 12a). The T-r_e plot (Fig. 12b) is utterly different from that for the deep continental clouds growing in smoke over the Amazon (Fig. 10b) but quite similar to the plot for the deep maritime clouds over the Amazon (Fig. 11b). Already at cloud base, r_e exceeds the precipitation threshold of 14 microns. There is no zone of diffusional

growth and the zone of coalescence extends from cloud base to 11°C. The rainout zone extends from 11°C to –5°C and the mixed-phase zone from –5°C to –12°C. Glaciation is complete at T < -12°C, which is even a little colder than the Amazon maritime case.

The vertical cross section of the clouds along the line in area 2 of Fig. 12a (Fig. 12c) is different from the vertical cross section taken through the continental clouds, which showed strong reflectivities extending to great heights. As with the Amazon maritime case, the extremely maritime clouds show the strongest reflectivities (>40 dBZ) below 5 km and the precipitation echoes average about 3 km below the visible cloud tops (Fig. 12c). This is due to the early formation and fallout of precipitation sized particles, which deplete the upper portions of the clouds of water and thus of large and highly reflective particles. Differences in vertical velocities, which are typically stronger in continental clouds, can explain some of the observed differences. However, no dynamical difference can explain the total lack of precipitation from polluted tropical convective clouds that do not exceed the freezing level, and certainly they would not undergo rainout if they grew to cumulonimbus stature. These differences in cloud and echo structure, which may due in part to differences in vertical velocity, can explain the lack of lightning discharges in maritime clouds (Zipser and Lutz, 1994).

These physical insights to the cloud and precipitation processes can be the basis for a large number of applications beyond those already mentioned in the qualitative part (Section 4.3 of this paper), including:

- Quantitative estimation of precipitation from clouds not detectable by any other satellite method, including passive microwave, which is not sensitive to warm rain and weak to moderate precipitation of any kind over land (see Lensky and Rosenfeld, 1997).
- Detection of severe storms, based on the depth and microstructure of the convective cloud elements.
- Detection of the impact of air pollution on the precipitation forming processes, as done already by Rosenfeld (1999, 2000).

- Application to cloud seeding for precipitation enhancement. The identification of regions containing clouds with ample supercooled water and inefficient precipitation processes can be used for evaluating the potential for added precipitation by cloud seeding, and for directing the cloud seeding operations. Furthermore, the seeding signature can be identified as microphysical changes in the seeded clouds, as shown by Woodley et al. (2000). The observed cloud microstructure is a manifestation of the aerosols and instability of the air mass, which are both slowly changing properties. Therefore, characterization of the cloud microstructure, as obtained from an orbital satellite, is still quite useful in spite of the scarcity of the satellite overpasses, because it is valid for at least several hours from the time of the observation.
- Application to cloud seeding for hail suppression. The identification of clouds with dynamical and microphysical structure conducive for hail can be used for directing the hail suppression operations of cloud seeding. The experience shows that a window of 25X25 1-km pixels is sufficient for the analyses of small convective clusters. In cases of seeded clouds it is quite practical to seed most of the towers in such an area, and create a seeding signature (Rosenfeld et al., 2001). The microphysical changes in the clouds due to seeding can be monitored and detected as well, as shown in Fig. 13.

5.0 Scientific Potential

5.1 Documentation of the Effect of Smoke on Cloud Processes

Besides addressing the method and its use and validation, the paper by Rosenfeld and Lensky (1998) deals with a matter of global import in suggesting that the smoke from the burning of biomass on a large-scale can suppress the regional rainfall from clouds ingesting the smoke.

A follow-up paper (Rosenfeld, 1999) made use of TRMM radar data to show unequivocally that the smoke from the fires in Indonesia and Malaysia in the deep tropics did indeed suppress the regional rainfall. The TRMM satellite was crucial to these

findings. The VIRS sensors were used to determine that both coalescence and ice processes were suppressed in the clouds ingesting the smoke and TRMM radar was used to show that rainfall was suppressed in the region of smoke.

5.2 The effect of urban and industrial pollution on clouds

Not much is known about the impact of aerosols from urban and industrial air pollution on precipitation. As was the case with the smoke from burning vegetation, it was assumed initially that industrial and urban pollution inhibited precipitation (Gunn and Phillips, 1957). However, later reports of enhanced rainfall downwind of paper-mills (Eagen et al., 1974) and over major urban areas (Braham, 1981) suggested that giant CCN caused enhancement of the precipitation (Johnson, 1982), but attempts to correlate the urban-enhanced rainfall to the air pollution sources failed to show any relationship (Gatz, 1979). The most plausible explanation for the urban rain enhancement invokes the heat-island effect and increased friction, both of which would tend to increase the surface convergence, resulting in more cloud growth and rainfall over and downwind of the urban areas. On the other hand, the recent suggestion published in "Nature" (Cerveny and Balling, 1998) that air pollution might enhance precipitation on the large scale in the northeastern U.S. and Canada and the speculative explanations for this effect would appear to confuse the issue. The truth is rather little is known definitively about this subject.

Space-borne measurements of ship tracks in marine stratocumulus provided the first evidence that effluents from ship stacks change cloud microstructure such that their water is redistributed into a larger number of smaller droplets (Coakley et al., 1987). Extrapolation of these observations to clouds that are sufficiently thick for precipitation (i.e., at least 2 km from base to top) would mean that the effluents have the potential to suppress precipitation.

Application of the imaging scheme of Rosenfeld and Lensky 1998) to the Advanced Very High Resolution Radiometer (AVHRR) onboard the National Oceanic

and Atmospheric Administration (NOAA) orbiting weather satellites have now revealed numerous "ship-track" like features in clouds over land, emanating from major urban and industrial pollution sources. These tracks are evident only in the near-infrared images with no hint of them in the visible images. Because the tracks evidently originate from pollution sources, they are named hereinafter "pollution tracks." Such tracks in the clouds have been illustrated downwind of Istanbul, Turkey, in Canada and downwind of major metropolitan and industrial areas in Australia (see Rosenfeld, 2000). In addition, pollution tracks have been noted (not shown) by Rosenfeld and Woodley downwind of Houston, Texas, over Manila Bay downwind of Manila, Philippines, near Guadalajara and Monterey, Mexico, downwind of Seattle, Washington, and Winnipeg, Canada. The longer one looks the more such tracks are found. Pollution tracks seem to be a global phenomenon.

Most of the pollution tracks were detected readily because there were pristine unpolluted areas of cloud nearby. This is illustrated in the image at 20:12 GMT on 20 July 1998 (Fig. 16) showing five pollution tracks in north-central Manitoba, Canada. These pollution plumes can be seen streaming to the south, staining the pristine cloud deck. The T-r_e plots for three of the stronger pollution tracks and for three unpolluted areas between the tracks are given in Fig. 17. The three plots for the unpolluted areas have effective radii that exceed the 14-micron precipitation threshold whereas the plots for the polluted areas have effective radii averaging 10 microns or less.

Farther south of the Canada pollution sources the unpolluted regions become harder to find. This is illustrated in the AVHRR image for the Great Lakes industrial area at 20:07 GMT on 5 June 1998 (Fig. 18). The yellow and orange coloration suggests that the effective radius is small in this region and this is verified by the T-R_e plots (Fig. 19) for the four areas shown in Fig. 18. Note that r_e averages 6 to 10 microns between $+2^oC$ and -10^oC. These values are similar to those found in the discrete pollution plumes farther north in Canada; only now the pollution is nearly continuous.

All of this is anecdotal, however, and does not make a quantitative case for the suppression of the rainfall by anthropogenic pollution. Rosenfeld (2000) made such a case for pollution tracks in Australia. Satellite retrievals of cloud microstructure clearly revealed plumes, embedded in extensive cloudy areas, in which the clouds contained small particle sizes. These plumes originated from major urban areas and industrial facilities such as power plants. The satellite retrievals in the polluted and unpolluted regions showed no coalescence in the polluted region and strong coalescence in the pristine clouds. In addition, the TRMM/PR revealed that the plumes of polluted clouds were devoid of precipitation, whereas the ambient clouds had precipitation intensities exceeding 10 mm/hr. Although producing no precipitation, the clouds in the plumes were as thick as the adjacent precipitating clouds and had no shortage of water. In addition, the PR detected a "bright band" signature, which is indicative of melting snow, in the adjacent precipitating unpolluted clouds, suggesting further that the pollution also suppresses the processes leading to the growth of ice particles to precipitation size.

It is suggested that the pollution suppresses precipitation in the same way as does smoke from burning vegetation. The ingested pollution aerosols nucleate many small cloud droplets, which remain small, thereby suppressing both warm rain processes and the formation and proliferation of ice in the clouds.

5.3 Measurement of Supercooled Water to near –38^{o}C

Adding to the credibility of the present satellite methodology was the discovery of large quantities (up to 1.9 gm/m^3) of supercooled cloud liquid water to near –38^{o}C (Fig. 14a). The slow growth of cloud droplets with height (Fig. 14b) and their large concentrations (Fig. 14c) show that under these conditions both warm and ice precipitation processes are suppressed. The measurements were made in Texas on 13 August 1999 by the authors with an instrumented cloud-physics jet aircraft in an attempt to validate the inferences by the present satellite methodology using TRMM data of supercooled liquid water to near the point of homogeneous nucleation.

The T-r_e plots for the TRMM satellite overpass at 22:45 GMT (1745 CDT) on 13 August 1999 are provided in Fig. 15. This is within 10 minutes of the time the liquid water measurements were made from the jet aircraft. Note that the r_e increased steadily with decreasing T until –38°C, indicating that only at that temperature were the clouds mostly glaciated. Thus, the satellite inferences and the in situ validation measurements were in general agreement on this day. Similar coincident measurements took place two days before, on 11 August 1999 (not shown), where the in situ and TRMM measured glaciation temperatures were –36°C and –38°C, respectively. Without the validating cloud physics measurements, however, it is doubtful that the satellite inferences would have been believed.

The authors made similar satellite and aircraft measurements near Mendoza, Argentina in January and February 2000 and observed supercooled cloud water contents up to 4 g m^{-3} near –38°C in Argentine clouds. Again, these aircraft measurements agreed with the indications from the satellite imagery.

6.0 Discussions

The Australian study is the first documented case linking urban and industrial air pollution to the reduction of the precipitation, pinpointing both the sources and the affected clouds. It was made possible by the newly acquired capabilities to observe both cloud microstructure and precipitation over large areas from the TRMM satellite. It might seem strange that some of the most obvious pollution signatures occur in Australia, which is probably the least polluted inhabited continent. The pollution signature on rainfall is most evident in Australia, perhaps because it is seen against a background of pristine clouds, whereas in most other places, such as the areas surrounding the Great Lakes in the U.S. and Canada (see previous section), the clouds are already polluted on a very large scale.

The results of the Australian and Indonesian cases are consistent with the findings of Gribbin (1995) indicating a decrease of rainfall in the tropics. A look at multi-spectral satellite data over the past couple of years suggests, however, that cloud microstructure and rainfall is being affected comparably by pollution over many other regions over the globe, including the tropics.

An intriguing case in point is the disparity in rainfall between the African Congo and the Amazon Basin of South America even though satellite rainfall estimates for the two regions, based on their infrared (IR) presentations and on passive microwave rainfall algorithms, are comparable (McCollum et al., 1999). Rainfall is nearly 50% less in the Congo than in the Amazon Basin. The rainfall from Congo clouds might be less than the rainfall from Amazon clouds because they have: a) less precipitable water with which to work, and/or b) lesser precipitation efficiency, and/or c) weaker forcing.

McCollum et al. (1999) used the present satellite technique to produce frequency plots for effective cloud radii (r_e) in the African Congo and the Amazon Basin (Fig. 20). Note the Amazon plot is shifted substantially toward larger effective radii relative to the plot for the Congo. As mentioned earlier, an effective radius threshold of 14 microns (Rosenfeld and Gutman, 1994) is used typically to identify which clouds have developed coalescence and are precipitating and which are not. Examining the areas under the curves in Fig. 20, it appears Amazon clouds in the sample have at least some coalescence over 90% of the time while the coalescence frequency for Congo clouds is about 50%. This is a large difference.

McCollum et al. (1999) have already suggested the possibility that the Congo vs. Amazon rainfall differences are, at least in part, due to less efficient clouds over the Congo, which are not able to form raindrops by coalescence as readily as the clouds over the Amazon. The microphysical observations of McCollum et al. (1999) are far from being climatologically representative for the whole area and all seasons. Therefore, they cannot be used as evidence that the indicated differences in the rainfall between central Africa and the Amazon are mainly due aerosol induced microphysical differences.

However, the new findings relating coalescence to rain production reported in Section 3.0 are consistent with this suggestion, as already made by McCollum et al. (1999) themselves. Although this could result from a number of causes, the nature of the CCN ingested by the clouds in the two regions is a plausible explanation. The air mass supplying Amazon clouds comes typically from the Caribbean and Atlantic and is likely more "maritime" in terms of the sizes and concentrations of the input CCN than the source of air for Congo clouds, which includes the Sahara, east Africa and the Kalahari deserts in addition to the Atlantic Ocean. The ingestion of anthropogenic pollution by the clouds in the African Congo also may play a role in the lesser precipitation efficiency relative to those in the Amazon.

This view is supported by the global plots of the Earth Probe TOMS Aerosol Index (Fig. 7). Virtually any other selection would have shown essentially the same pattern. Africa is an anomaly when it comes to pollutants and aerosols, especially on the northern and southern margins of equatorial Africa. There are almost always fires and dust storms on the fringes of the intertropical convergence zone and they move north and south with the seasons. One can readily imagine these aerosols being drawn toward the equator into the migratory weather disturbances that move from east to west across the African continent much of the year. These aerosols certainly have the potential to influence the rainfall. The Amazon Basin on the other hand has less aerosol pollution relative to Africa, although the example presented in Fig. 7 is one of the exceptions. It seems possible, therefore, that the natural and anthropogenic aerosols are acting to decrease the rainfall over tropical Africa.

Collectively, the Amazon Basin and the African Congo constitute a significant fraction of the world's deep tropics. If natural and/or anthropogenic pollution is shown to account for the differences in rainfall and lightning between the two regions, its effect on climate might be quantified through computer simulations

Until this is done, we will have to live with the clear implications that smoke from biomass burning and from urban and industrial sources are highly detrimental to the

efficiency of both water and ice precipitation forming processes in convective clouds. The resulting excess water vapor remaining in the atmosphere may eventually precipitate elsewhere, causing redistribution of the large-scale precipitation and latent heating, which means alterations of the driving force behind atmospheric circulations. Hence, the question arises whether microphysical processes can influence large scale or even global climate.

Aircraft validation of satellite inferences of deep supercooling in vigorous convective clouds has implications for the modeling of convective clouds, for deliberate modification of cloud processes and for studies of global climate. The validation has been made in Texas and Argentina, but the satellite imagery indicates that such supercooling takes place over many other regions in the world. This would seem to fly in the face of conventional wisdom and at variance with most modeling simulations that show glaciation in continental convective clouds at warmer temperatures. For example, full glaciation was parameterized to occur naturally at –20^{o}C in clouds in HIPLEX (Orville, 1996), which took place in the same area where the clouds were shown to fully glaciate only at –38^{o}C (Rosenfeld and Woodley, 2000). This supercooling indicates that such clouds have low precipitation efficiency and may be good candidates for seeding intervention.

Deep supercooling is also probably a manifestation of feedback from natural and anthropogenic pollution. Polluted clouds have suppressed coalescence and ice processes and likely are characterized by supercooling to great depths. If this is so, the convective clouds in tropical Africa must be much more supercooled than those in the South American Amazon. Such regional differences may be changing with time with implications for the global climate.

6.0 Conclusions

We are back where Joanne Simpson began, but with new tools and new insights. We know much more about microphysical processes in clouds. Maritime clouds are

much different from continental clouds. They ingest fewer aerosols, produce raindrops through coalescence and average up to 100% more rain volume per convective cell than continental clouds. Highly maritime clouds are poor candidates for both glaciogenic and hygroscopic seeding, because they produce raindrops at temperatures > 0^{o}C, which readily freeze at temperatures near –5^{o}C, producing ice splinters and rapid glaciation of the cloud. Continental clouds, on the other hand, have been shown to carry their cloud water in many cases to near –38^{o}C before freezing. Such clouds are highly inefficient and should be good candidates for glaciogenic and/or hygroscopic seeding intervention.

Pollution has a major impact on cloud processes. New satellite imagery and new methods to assimilate and analyze it have documented the microphysical structure of clouds over large space and time scales. This new look has demonstrated the profound impact that natural and anthropogenic aerosols have on the rain-forming processes in clouds. The implications are potentially enormous. The increasing pollution must be affecting global rainfall detrimentally. At the very least, pollution must be redistributing the rainfall.

Anthropogenic pollution from industry and urbanization also acts negatively on the rain-forming processes in clouds. In the cities this negative effect may be over-compensated by increased convergence and rainfall due to dynamic factors, including the "heat island" and increased surface roughness from the clustering of large structures (Braham, 1981). Away from these dynamic enhancements, however, the effect of pollution on rainfall should be negative. It is quite possible, therefore, that the combination of smoke from burning vegetation, urban and industrial pollution is having an effect on the global climate by decreasing and/or redistributing the rainfall, especially where precipitation originates from convective clouds. This has serious potential implications for the availability of water resources, which might be compromised, especially in the most densely populated areas of the tropics and subtropics, where people are dependent on these waters for their livelihood.

The changes in precipitation distribution must be associated with respective changes in latent heat release, which drives the global circulation. Therefore, a change in the global circulation is a likely outcome. If so, these changes are already with us today, and the climate system would have been different without today's anthropogenic emissions of aerosols.

In getting back to where we started, we have learned much along the way. Tropical convective clouds are just as important to the world climate as they were when Joanne Simpson began her illustrious meteorological career, but other factors have intervened. Our results, and those of METROMEX years ago, indicate that inadvertent weather modification is a reality (Braham, 1981). The more we look the more prevalent it appears to be. The challenge now is to understand and quantify its extent and its effect on clouds, precipitation, and on local and global climates. Deliberate weather modification through cloud seeding pales in comparison to the modifications being accomplished inadvertently, and it may some day have to be employed to offset the unintended modifications (e.g., hygroscopic seeding of clouds to offset the detrimental effects of pollution on rain-forming processes). Many of the past advances in cloud physics technology and insights have been made in the context of cloud seeding experiments. Future progress is likely to be accelerated now that pollution and its probable effect on the global climate has been brought to the attention of the scientific community.

Acknowledgments

We offer a special thanks to Dr. Joanne Simpson for her help and inspiration through the years. We have seen time and again in our trek through life how much difference just one person can make in the lives of others. Joanne was that person in our professional lives. Because words often fail us, as in this acknowledgment, we have produced this paper in her honor in the hope that it will provide her some excitement and new ways to look at the meteorological problems that have intrigued her during her distinguished career.

This study was partially funded by the Israeli Space Agency.

REFERENCES

Arking, A., and J. D. Childs, Jeffrey D., 1985: Retrieval of cloud cover parameters from multispectral satellite images. Journal of Climate and Applied Meteorology, Boston, 24(4): 322-333.

Bigg, E.K. , 1953: The formation of atmospheric ice crystals by the freezing of droplets. *Quart. J. Roy. Meteor. Soc.*, **79**, 510-519.

Biswas, K. R., and A. S. Dennis, 1971: Formation of rain shower by salt seeding. *J. Appl. Meteor.,* **10,** 780–784.

Bowen, E. G., 1952: A new method of stimulating convective clouds to produce rain and hail. *Quart. J. Roy. Meteor. Soc.,* **78,** 37–45.

Braham, R. R., Jr., 1964: What is the role of ice in summer rain showers? *J. Atmos. Sci.,* **21,** 640–645.

Braham, Roscoe R., Jr., 1981: Summary of urban effects on clouds and rain. *Meteorological Monographs*, Boston, **18**(40): 141-152.

Cerveny R S, and R C Balling Jr, 1998: Weekly cycles of air pollutants, precipitation and tropical in the coastal NW Atlantic region (Letter to Nature). *Nature*, **394**, No 6693, 561-563.

Coakley, J. A., R. L. Bernstein, and P. R. Durkee, 1987: Effects of ship-stack effluents on cloud reflectivity. *Science,* **237,** 1020-1022.

Cotton, W. R., 1982: Modification of precipitation from warm clouds—A review. *Bull. Amer. Meteor. Soc.,* **63,** 146–160.

Cooper, W. A., R. T. Bruintjes, and G. K. Mather, 1997:. Calculations pertaining to hygroscopic seeding with flares. *J. Appl. Meteor.*, **36,** 1449-1469.

Eagen, R. C., P. V. Hobbs, and L. F. Radke, 1974: Particle emissions from a large Kraft paper mill and their effects on the microstructure of warm clouds. *Journal of Applied Meteorology*, **13**(5):535-552.

Gatz, Donald F., 1979: Investigation of pollutant source strength rainfall relationships at St. Louis. *Journal of Applied Meteorology*, Boston, **18**(10): 1245-1251.

Gerber, H., 1996: Microphysics of marine stratocumulus clouds with two drizzle modes. *J. Atmos. Sci.*, **53**, 1649-1662.

Gribbin, J., 1995: Rain moves north in the global greenhouse. New Scientist, 4 March 1995, p18.

Gunn, R. and B. B. Phillips, 1957: An experimental investigation of the effect of air pollution on the initiation of rain. *J. Meteor*., **14**, 272-280.

Houghton, J. T., L. G. Meira Filho, J. Bruce, Hoesung Lee, B. A. Callander, E. Haites, N. Harris, and K. Maskell, 1994: Climate Change 1994 - Radiative forcing of climate change and an evaluation of the IPCC IS92 Emission Scenarios. Reports of working groups I and II of the Intergovernmental Panel on Climate Change. Cambridge University Press, 339p.

Johnson, D. B., 1982: Role of giant and ultragiant aerosol particles in warm rain initiation. *Journal of the Atmospheric Sciences*, **39**(2): 448-460.

Johnson, D. B., 1987: On the relative efficiency of coalescence and riming. *J. Atmos. Sci.,* **44,** 1671–1680.

Kaufman Y. J., and R. S. Fraser, 1997: The effect of smoke particles on clouds and climate forcing. *Science*, **277**(5332): 1636-1638.

Lensky I. M. and D Rosenfeld, 1997: Estimation of precipitation area and rain intensity based on the microphisical properties retrieved from NOAA AVHRR data. Journal of Applied Meteorology, 36, 234-242.

Mather, G.K., D.E. Terblanche, F.E. Steffens and L. Fletcher, 1997: Results of the South African cloud seeding experiments using hygroscopic flares. *J. Appl. Meteor.*, **36**, 1433-1447.

McCollum, J. A., A. Gruber, and M. B. Ba (1999): Discrepancy between gauges and satellite estimates of rainfall in equatorial Africa. Submitted to J. Appl. Meteor.

Nakajima, T., and M. D. King, 1990: Determination of the optical thickness and effective particle radius of clouds from reflected solar radiation measurments. Part I: Theory. *J. Atmos. Sci.,* **47,** 1878-1893.

Orville, H. D., 1996: A review of cloud modeling in weather modification. Bulletin of the American Meteorological Society, Boston, MA, 77(7): 1535-1555.

Pinsky M. B., A. P. Khain, D. Rosenfeld, and A. Pokrovsky, 1998: Comparison of collision velocity differences of drops and graupel particles in a very turbulent cloud. *Atmos. Res.*, **49**, 99-113.

Radke, L. F., J. A. Coakley, and M. D. King, 1989: Direct and remote sensing observations of the effects of ships on clouds. *Science,* **246**, 1146-1149.

Reisin, T., S. Tzivion, and Z. Levin, 1996: Seeding convective clouds with ice nuclei or hygroscopic particles: a numerical study using a model with detailed microphysics. *J. Appl. Meteor.,* **35**, 1416-1434.

Rosenfeld, D., D. B.Wolff, and D. Atlas, 1993: General probability-matched relations between radar reflectivity and rain rate, J. Appl. Meteor., 32, 50-72.

Rosenfeld, D. and W.L. Woodley, 1993: Effects of cloud seeding in west Texas: Additional results and new insights. J. Appl. Meteor., **32**, 1848-1866.

Rosenfeld, D., and G. Gutman, 1994: Retrieving microphysical properties near the tops of potential rain clouds by multispectral analysis of AVHRR data. *J. Atmos. Res.,* 34, 259-283.

Rosenfeld, D. and M.I. Lensky, 1998: Space-borne based insights into precipitation formation processes in continental and maritime convective clouds. *Bull. Amer. Meteor. Soc.*, **79**, 2457-2476.

Rosenfeld D., 1999: TRMM Observed First Direct Evidence of Smoke from Forest Fires Inhibiting Rainfall. Geophys. Res. Lett., 26, No. 20, 3105.

Rosenfeld D., 2000: Suppression of Rain and Snow by Urban and Industrial Air Pollution. *Science*, **287** (5459), 1793-1796.

Rosenfeld D. and W. L. Woodley, 2000: Convective Clouds with Sustained Highly Supercooled Liquid Water Down to –37.5^{o}C. *Nature*, **405**, 440-442.

Rosenfeld D. and W. L. Woodley, and T. Krauss, 2001: Satellite Observations of the Microstructure of Natural and Seeded Severe Hailstorms in Argentina and Alberta. *15th Conference on Planned and Inadvertent Weather Modification*. AMS, 14-18 January 2001, Albuquerque, New Mexico, p. 68-74.

Schickel, K. P, H. E. Hoffmann, and K. T. Kriebel, 1994: Identification of icing water clouds by NOAA AVHRR satellite data. Atmospheric Research, Amsterdam, The Netherlands, 34(1-4): 177-183.

Simpson, J., G.W. Brier and R.H. Simpson, 1967: Stormfury cumulus seeding experiment 1965: Statistical analysis and main results. J. Atmos. Sci., 24, 508-521.

Simpson, J., 1980: Downdraft as linkages in dynamic cumulus seeding effects. J. Appl. Meteor., 19, 477-487.

Simpson, J. and W. L. Woodley, 1971: Seeding cumulus in Florida: New 1970 results. Science, 173, 117-126.

Squires, P., 1958: The microstructure and colloidal stability of warm clouds. *Tellus* **10**, 256-271.

Twomey, S., R.Gall, and M. Leuthold, 1987: Pollution and cloud reflectance. Boundary Layer Meteorology, Dordrecht, Holland, Special Issue, 41(1/4): 335-348, Oct./Dec., 1987.

Witt. G. and J. Malkus, 1959: The evolution of a convective element: A numerical calculation. *The Atmosphere and the Sea in Motion*. Rockefeller Institute, Oxford University Press, 425-439, 1959.

Woodley, W., and Herndon, A. 1970. A Raingauge Evaluation of the Miami Reflectivity-Rainfall Rate Relation. *Journal of Applied Meteorology* **14**: 909-28.

Woodley, W.L., J. Jordan, J. Simpson, R. Biondini, J.A. Flueck and A. Barnston, 1982: Rainfall results of the Florida Area Cumulus Experiment. J. Appl. Meteor., **21**, 139-164.

Woodley, W.L., A.G. Barnston, J.A. Flueck, and R. Biondini, 1983: The Florida Area Cumulus Experiment's second phase (FACE-2). Part II: Replicated and confirmatory analyses. A. Appl. Meteor., **22**, 1529-1540.

Woodley W. L., D. Rosenfeld, and A. Strautins, 2000: Identification of a seeding signature in Texas Using Multi-Spectral Satellite Imagery. J. Wea. Mod., **32**, 37-51.

Zipser J., E., and K. R. Lutz, 1994: The vertical profile of radar reflectivity of convective cells: a strong indicator of storm intensity and lightning probability?. *Monthly Weather Review*, **122**, 1751-1759.

List of Captions

Fig. 1. The mean rain volumes of convective cells as a function of maximum precipitation echo top height for cells growing on days with weak coalescence activity (Category 1) and on days with strong coalescence activity (Category 2). The data are plotted at the center point of 2 km intervals of maximum echo top height. For the purpose of showing the trend on a logarithmic scale, a value of 10^2 m^3 was used instead of the zero value of RVOL for the 3 km maximum echo top height interval for cells growing on days with weak coalescence activity (Category 1).

Fig 2. Mean rain-volume differences (dashed line) and ratios of mean rain volumes (solid curve) versus maximum precipitation echo top height for cells growing on days with weak coalescence activity (Category 1) and on days with strong coalescence activity (Category 2). The data are plotted at the center point of 2 km intervals of maximum echo top height. For the purpose of showing the trend on a logarithmic scale, a value of 10^2 m^3 was used instead of the zero value of RVOL for the 3 km maximum echo top height interval for cells growing on days with weak coalescence activity (Category 1).

Fig. 3: The relation of the spectral bands of the Meteosat Second Generation (MSG) satellite with respect to the top-of-the-atmosphere solar and surface terrestrial radiation fluxes. Note that the 3.8 μm channel receives both solar and thermal radiation, and it is on the common minimum. Therefore, thermal emission must be deducted in obtaining solar reflectance at 3.8 μm.

Fig. 4: The dependence of the absorption coefficients of water and ice on wavelength. The MSG channels in the atmospheric windows are denoted. Note that water and ice are practically non-absorbing in the visible, and strongly absorbing at 3.8 μm. The ice absorbs much more strongly than water at 1.6 μm. This makes 1.6 μm useful for separating ice from water clouds and surfaces.

Fig. 5: Ship tracks over the North Pacific, as observed by the NOAA/AVHRR on 22 June 2000, 03:25 GMT. The color scheme is red for the visible, green for 3.7 μm reflectance component, and blue for temperature. The ship tracks with reduced particle size appear as cloud bands of enhanced green, or enhanced 3.7 μm reflectance. For full description of the color table see Table 2.

Fig. 6**:** The classification scheme of convective clouds into microphysical zones, according to the shape of the T-r_e relations. Note that in extremely continental clouds r_e at cloud base is very small, the coalescence zone vanishes, mixed phase zone starts at T<-15^{o}C, and the glaciation can occur in the most extreme situation at the height of homogeneous freezing temperature of –39^{o}C. In contrast, maritime clouds start with large r_e at their base, crossing the precipitation threshold of 14 μm a short distance above the base. The deep rainout zone is indicative of fully developed warm rain processes in the maritime clouds. The large droplets freeze at relatively high temperatures, resulting in a shallow mixed-phase zone and a glaciation temperature reached near –10^{o}C.

Fig 7a: Wave clouds in area of about 300x200 km in the lee of the Andes, forming as supercooled water cloud at their leading edge (upper left edge of the waves), as evident by the yellow color (see Table 2 for color interpretation). The image was taken by the NOAA/AVHRR on 7 January 1999, 20:08 GMT. Abrupt freezing occurs at –32^{o}C, as indicated by the red color and the jump to a larger indicated effective radius at –32^{o}C, as shown in Fig. 7b.

Fig. 7b: The T-r_e for frame 7a. The microphysical zones are marked by the vertical bars where 1 = diffusional growth, and 5 = glaciated. Note that glaciation is indicated at –32^{o}C.

Fig. 8: Earth Probe TOMS Aerosol Index on 13 September 1998, showing the smoke from forest fires in the Amazon and Congo basins.

Fig. 9a: A TRMM image showing microphysically continental cumulus clouds growing in smoke over the Amazon, centered at 15^{o}S, 60^{o}W, at 19:15 GMT on September 13, 1998. The 230 km radar swath is delimited between the white lines. The white hatching is areas with radar-detected precipitation. The yellow crosses are lightning flashes, as detected by the TRMM/LIS. The color scheme is given in Table 2.

Fig. 9b: The T-r_e for frame 1 of Fig. 9a. The microphysical zones are marked by the vertical bars where 1 = diffusional growth, 2 = coalescence, and 4 = mixed phase zones. The lines for the 15th, 50th and 85th percentiles of pixels having r_e for a given T are plotted. Note that the 14-micron precipitation threshold is reached only at T<-10^{o}C.

Fig. 9c: The vertical cross section of the clouds along the lines in Fig. 9a. The two cross sections are delimited by the same characters in this figure and in Figure 9a. Note that clouds reaching tops < 7 km do not precipitate.

Fig. 10a: A TRMM image showing microphysically continental cumulus and cumulonimbus clouds growing in smoke over the Amazon, centered at 13^{o}S, 61^{o}W, on 18:16 GMT, September 15, 1998. The color scheme is given in Table 2.

Fig. 10b: The T-r_e for the frame in Figure 10a. The lines of the 15th, 50th and 85th percentiles of pixels with re for a given T are plotted. The microphysical zones are marked by the vertical bars where 1 = diffusional growth, 4 = mixed phase and 5 = glaciated. Note that glaciation is indicated at –27^{o}C.

Fig. 10c: The vertical cross section of the clouds along the line in Fig. 10a. Note that that the Z>40 dBZ extends to H=10 km, i.e., well above the 0^oC isotherm.

Fig. 11a: A TRMM image showing microphysically maritime cumulus and cumulonimbus clouds growing in clean air over the Amazon, centered at 5^oS, 59^oW, on 16:28 GMT on April 13, 1998. The color scheme is given in Table 2.

Fig. 11b: The T-r_e plot for the frame in Figure 11a. The microphysical zones are marked by the vertical bars 2 = coalescence, 3 = rainout, 4 = mixed phase and 5 = glaciated zones. Note the deep rainout zone and the glaciation indicated at the relatively high T=-7^oC.

Fig. 11c: The vertical cross section of the clouds along the line in Fig. 9a. Note that the shallowest clouds already precipitate. Also note that the Z>40 dBZ is confined to H<5 km, i.e., below the 0^oC isotherm.

Fig. 12a: A TRMM image showing microphysically maritime cumulus and cumulonimbus clouds over the equatorial Pacific near Kwajalein, centered at 6N 167W, on 02:51 GMT November 5, 1998. The color scheme is given in Table 2.

Fig. 12b: The T-r_e for the frame in Figure 12a. Note the great similarity of the microphysical zones to the clouds over the Amazon in the clean air, as shown in Figure 11b.

Fig. 12c: The vertical cross section of the clouds along the line in Fig. 12a. Note that the shallowest clouds already precipitate. Also note that the Z>40 dBZ is confined to H<5 km, i.e., below the 0^oC isotherm.

Fig. 13a**:** Hailstorm Cb clouds in an area of about 150x150 km over Alberta, Canada, as observed by the NOAA/AVHRR overpass of 10 July 1998 at 22:15 GMT. According to

the color classification scheme presented in Table 2, the yellow cumuliform cloud elements indicate they are composed of supercooled droplets. The red areas are the anvils of the Cb tops.

Fig. 13b: The T-r_e for frames 2 and 3 of Fig. 13a. The T- r_e graphs for area #2 shows very deep supercooled water and mixed phase clouds with glaciation occurring only at –37^{o}C. The same applies to Area 1 (not shown). The clouds in Area 3 were seeded with A_gI ice nuclei, and glaciated between –15 to –25^{o}C in different parts of the cloud, as indicated by the T- r_e graph for that area. Hail was observed in the area on that day. However, clouds 1 and 2 occurred over remote areas where there were no observations.

Fig. 14a: The supercooled cloud liquid water content as a function of temperature, in all the clouds on the 13 August 1999. Each point represents one second of measurements, or 150 - 200 m of cloud path. Note the abrupt decrease of the water at –38^{o}C, indicating the point of homogeneous freezing. The dotted curve marks the ½ adiabatic water content, as a reference for the rate of consumption of cloud water to freezing and other processes. The black dots are those in which the hot wire sensor detected less than 0.3 g m^{-3} liquid water contents.

Fig. 14b: The median volume diameter of the cloud particles measured by a Forward Scattering Spectrometer Probe (FSSP) as a function of temperature, in all the clouds on the 13 August 1999. Each point represents one second of data, or 150 - 200 m of cloud path, containing more than 100 cm^{-3} FSSP-measured cloud particles. The red symbols denote cloud segments with hot-wire measured liquid water contents $\geq$0.3 gm^{-3}.

Fig. 14c: The same as Fig. 2, but for the FSSP-100 measured concentration of cloud particles.

Fig. 15. The T-r_e plots for the TRMM satellite overpass at 22:45 GMT (1745 CDT) on 13 August 1999. The clouds profiled were those in which the aircraft measurements were

made. Note that the r_e increased steadily with decreasing T until about –38°C, indicating that only at that temperature were the clouds mostly glaciated.

Fig. 16: Processed AVHRR image at 2012 GMT on 20 July 2000 showing five pollution tracks in a supercooled cloud deck in north-central Manitoba Province, Canada. The dimensions of the image is 550X250 km.

Fig. 17: The effective radius in and outside of the pollution tracks shown in Fig. 16. The numbers in the figure correspond to the numbered areas in Fig. 16.

Fig. 18: The AVHRR image for the Great Lakes industrial area at 2007 GMT on 5 June 1998.

Fig. 19: The T-r_e plots for the four areas shown in Fig. 18. Note that r_e averages 6 to 10 microns between +2°C and –10°C.

Fig. 20: Plot of the relative frequency of effective cloud radius for clouds over the African Congo (black bars) and the Amazon (crosshatched bars). (After McCollum et al., 1999).

Appendix A:

Glossary:

AVHRR: Advanced Very High Resolution Radiometer onboard the NOAA satellites
CCN: Cloud Condensation Nuclei
EDOP: NASA's ER2-Doppler radar
ELDORA: NCAR Electra Doppler Radar
HIPLEX: High Plains Cooperative Experiment
LIS: TRMM Lightning Imaging Sensor
METEOSAT: European geostationary meteorological satellite
METROMEX: Metropolitan Meteorological Experiment
MODIS: Moderate Resolution Imaging Spectroradiometer
MSG: METEOSAT Second Generation
NASA: National Aeronautics and Space Administration
NCAR: National Center for Atmospheric Research
NOAA: National Oceanic and Atmospheric Administration
PR: TRMM Precipitation Radar
TOMS: Total Ozone Mapping Spectrometer
VIRS: TRMM Visible and Infra Red Sensor

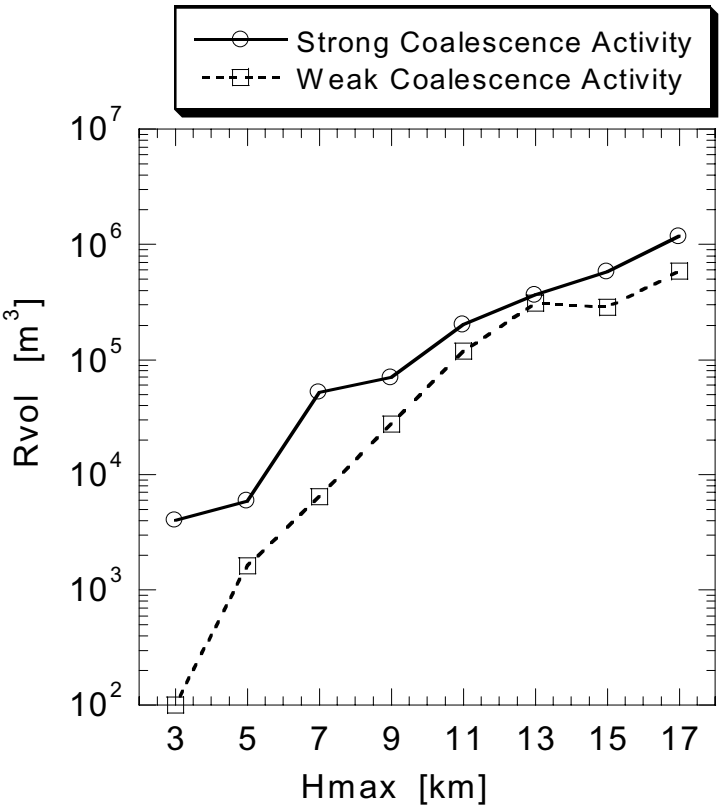

Fig. 1. The mean rain volumes of convective cells as a function of maximum precipitation echo top height for cells growing on days with weak coalescence activity (Category 1) and on days with strong coalescence activity (Category 2). The data are plotted at the center point of 2 km intervals of maximum echo top height. For the purpose of showing the trend on a logarithmic scale, a value of 10^2 m^3 was used instead of the zero value of RVOL for the 3 km maximum echo top height interval for cells growing on days with weak coalescence activity (Category 1).

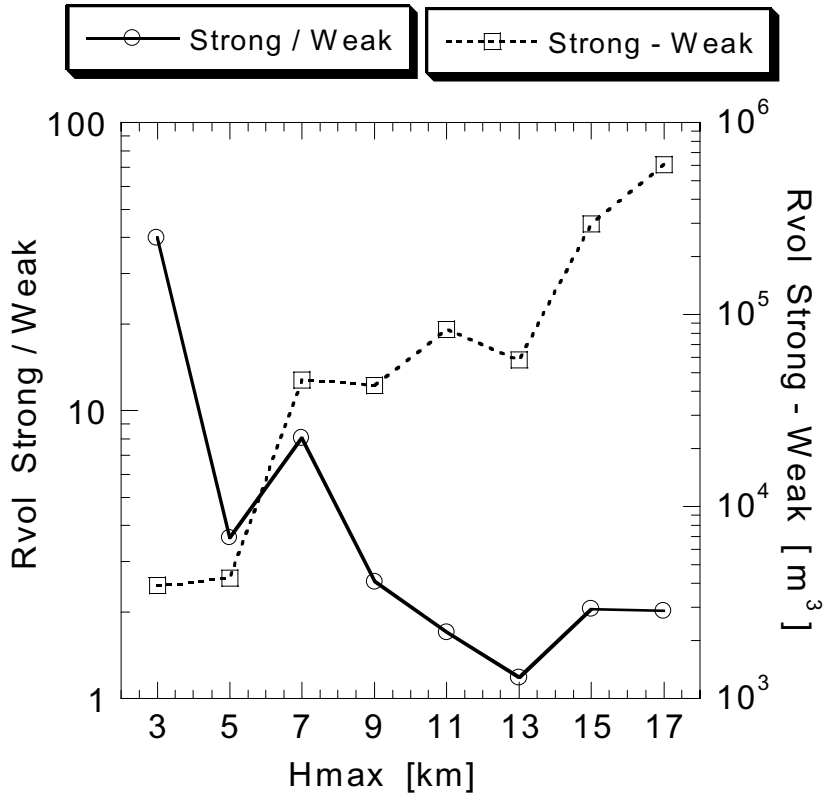

Fig 2. Mean rain-volume differences (dashed line) and ratios of mean rain volumes (solid curve) versus maximum precipitation echo top height for cells growing on days with weak coalescence activity (Category 1) and on days with strong coalescence activity (Category 2). The data are plotted at the center point of 2 km intervals of maximum echo top height. For the purpose of showing the trend on a logarithmic scale, a value of 10^2 m^3 was used instead of the zero value of RVOL for the 3 km maximum echo top height interval for cells growing on days with weak coalescence activity (Category 1).

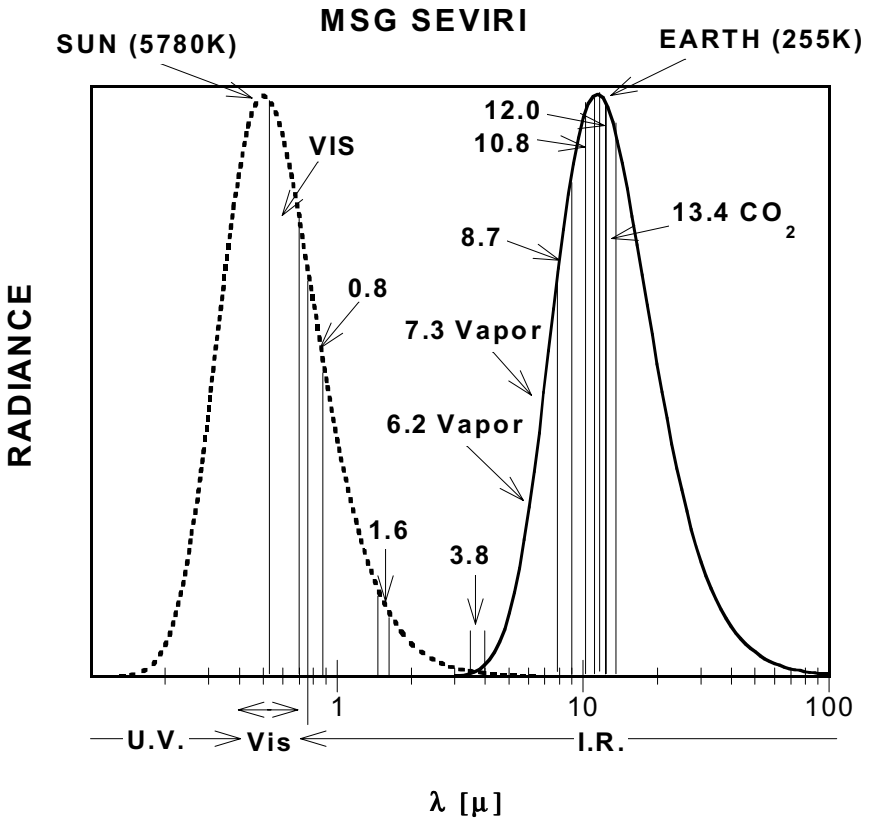

Fig. 3: The relation of the spectral bands of the Meteosat Second Generation (MSG) satellite with respect to the top-of-the-atmosphere solar and surface terrestrial radiation fluxes. Note that the 3.8 μm channel receives both solar and thermal radiation, and it is on the common minimum. Therefore, thermal emission must be deducted in obtaining solar reflectance at 3.8 μm.

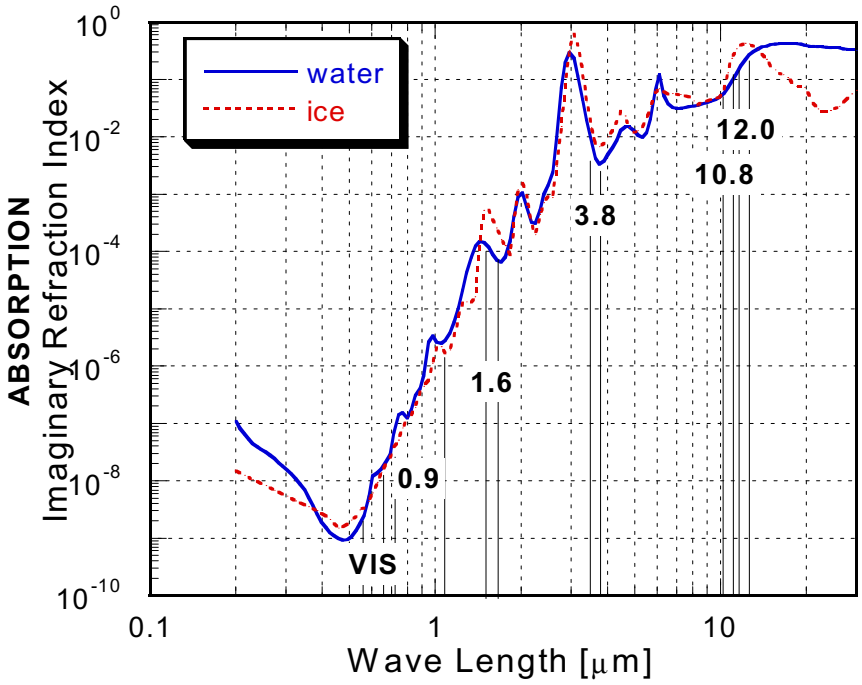

Fig. 4: The dependence of the absorption coefficients of water and ice on wavelength. The MSG channels in the atmospheric windows are denoted. Note that water and ice are practically non-absorbing in the visible, and strongly absorbing at 3.8 μm. The ice absorbs much more strongly than water at 1.6 μm. This makes 1.6 μm useful for separating ice from water clouds and surfaces.

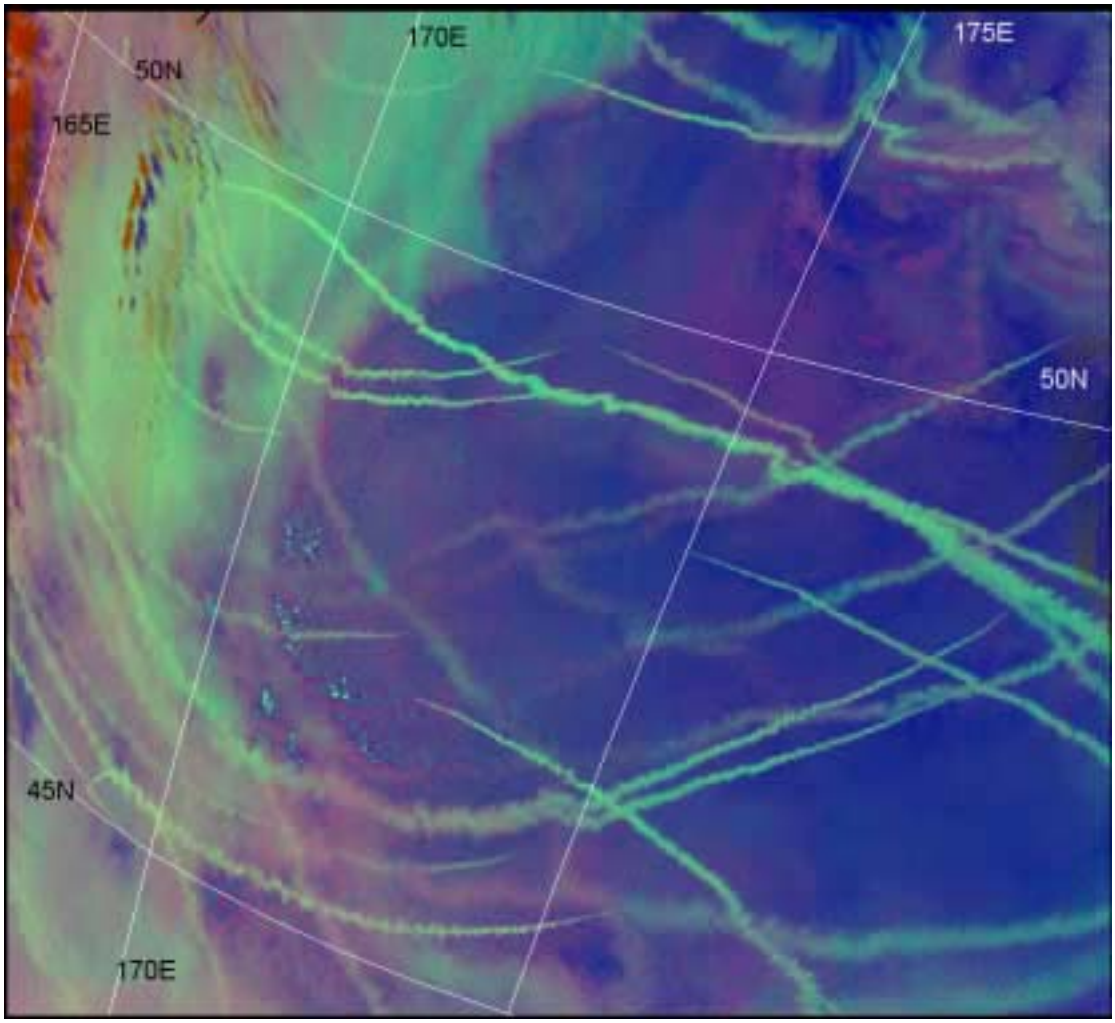

Fig. 5: Ship tracks over the North Pacific, as observed by the NOAA/AVHRR on 22 June 2000, 03:25 GMT. The color scheme is red for the visible, green for 3.7 μm reflectance component, and blue for temperature. The ship tracks with reduced particle size appear as cloud bands of enhanced green, or enhanced 3.7 μm reflectance. For full description of the color table see Table 2.

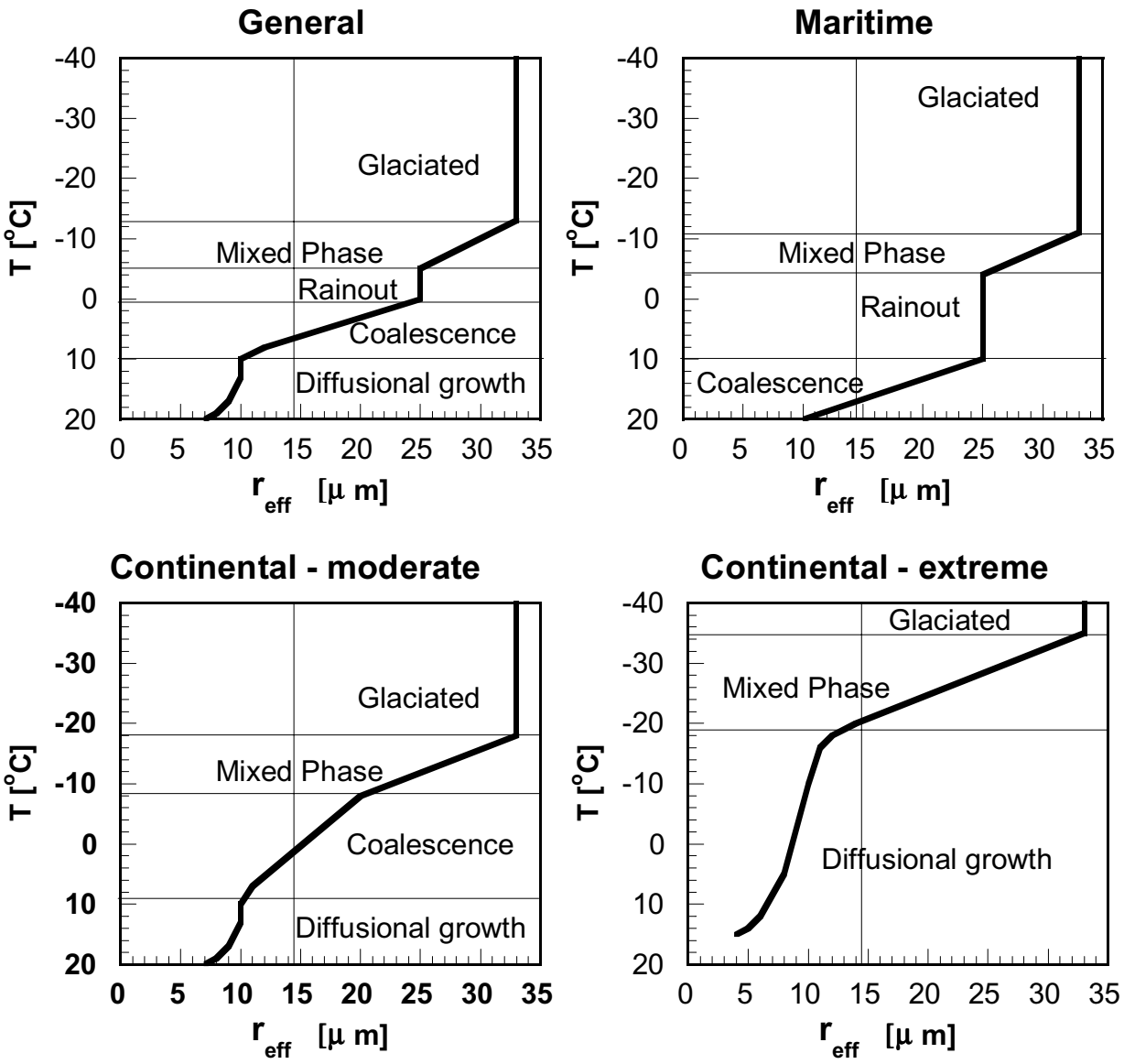

Fig. 6**:** The classification scheme of convective clouds into microphysical zones, according to the shape of the T-r_e relations. Note that in extremely continental clouds r_e at cloud base is very small, the coalescence zone vanishes, mixed phase zone starts at T<-15°C, and the glaciation can occur in the most extreme situation at the height of homogeneous freezing temperature of –39°C. In contrast, maritime clouds start with large r_e at their base, crossing the precipitation threshold of 14 μm a short distance above the base. The deep rainout zone is indicative of fully developed warm rain processes in the maritime clouds. The large droplets freeze at relatively high temperatures, resulting in a shallow mixed-phase zone and a glaciation temperature reached near –10°C.

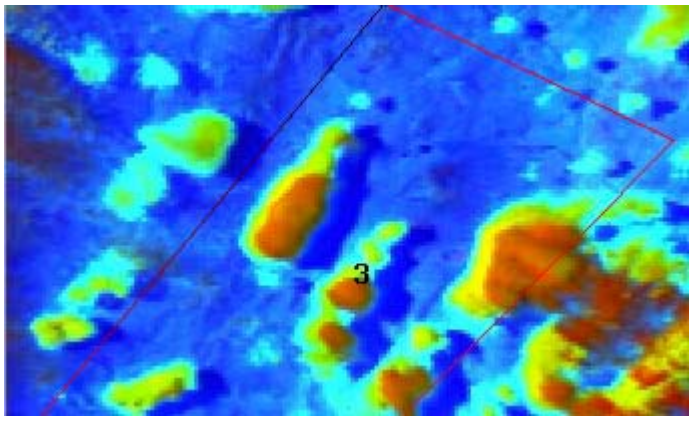

Fig 7a: Wave clouds in area of about 300x200 km in the lee of the Andes, forming as supercooled water cloud at their leading edge (upper left edge of the waves), as evident by the yellow color (see Table 2 for color interpretation). The image was taken by the NOAA/AVHRR on 7 January 1999, 20:08 GMT. Abrupt freezing occurs at –32°C, as indicated by the red color and the jump to a larger indicated effective radius at –32°C, as shown in Fig. 7b.

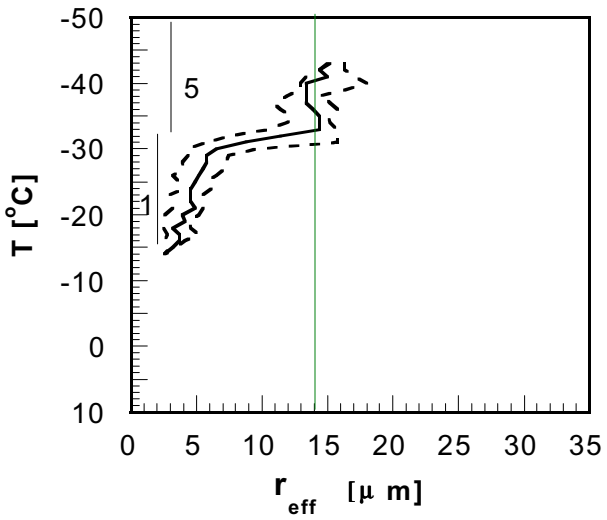

Fig. 7b: The T-r_e for frame 7a. The microphysical zones are marked by the vertical bars where 1 = diffusional growth, and 5 = glaciated. Note that glaciation is indicated at –32°C.

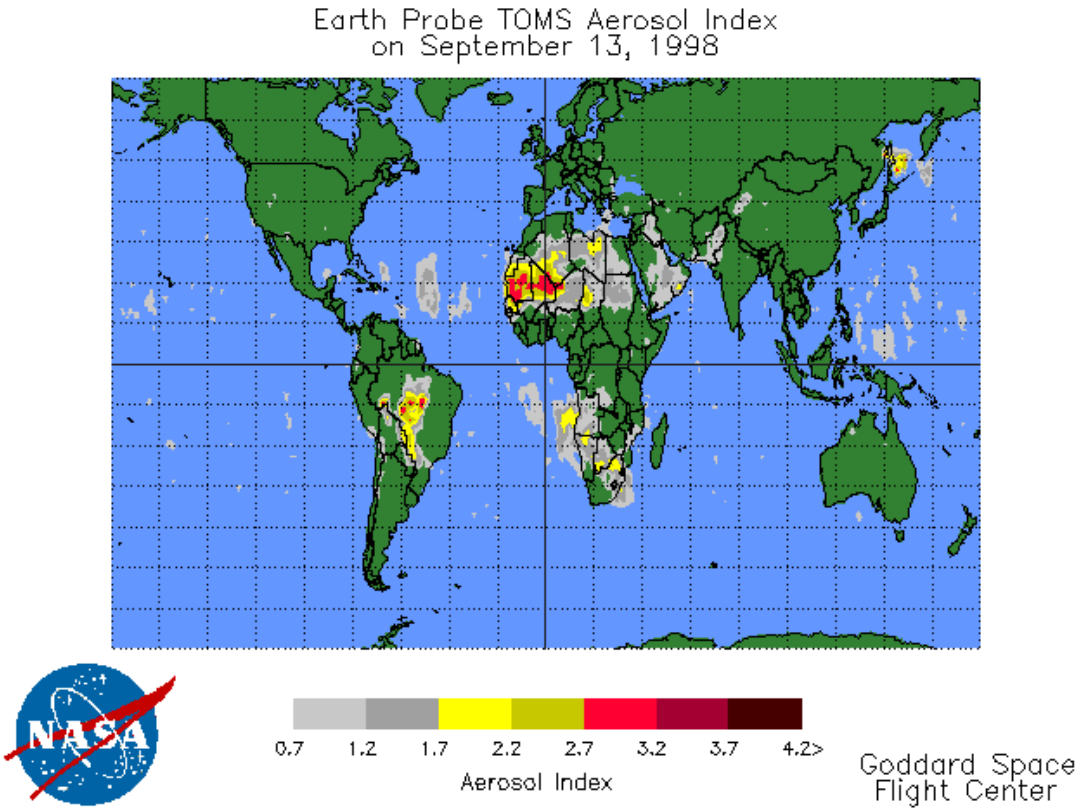

Fig. 8: Earth Probe TOMS Aerosol Index on 13 September 1998, showing the smoke from forest fires in the Amazon and Congo basins.

Fig. 9a: A TRMM image showing microphysically continental cumulus clouds growing in smoke over the Amazon, centered at 15°S, 60°W, at 19:15 GMT on September 13, 1998. The 230 km radar swath is delimited between the white lines. The white hatching is areas with radar detected precipitation. The yellow crosses are lightning flashes, as detected by the TRMM/LIS. The color scheme is given in Table 2.

.

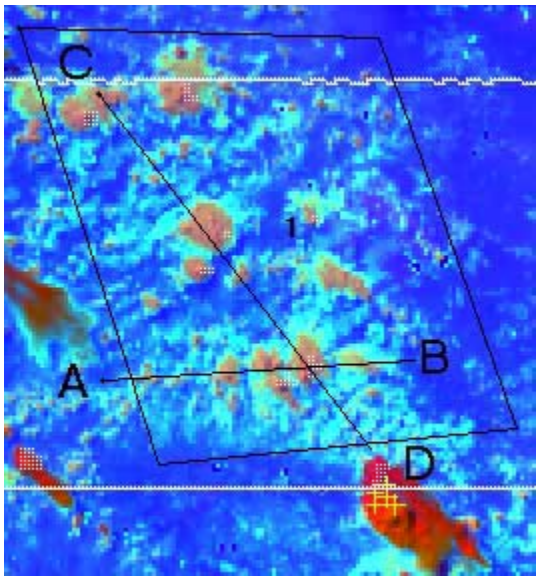

Fig. 9b: The T-r_e for frame 1 of Fig. 9a. The microphysical zones are marked by the vertical bars where 1 = diffusional growth, 2 = coalescence, and 4 = mixed phase zones. The lines for the 15th, 50th and 85th percentiles of pixels having r_e for a given T are plotted. Note that the 14-micron precipitation threshold is reached only at T<-10°C.

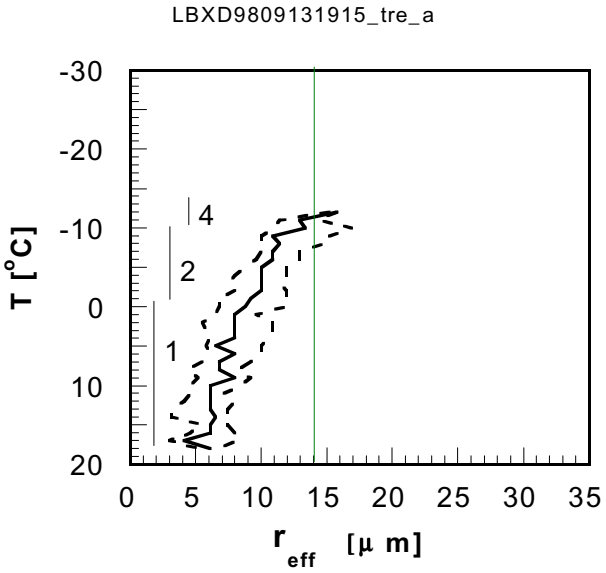

Fig. 9c: The vertical cross section of the clouds along the lines in Fig. 9a. The two cross sections are delimited by the same characters in this figure and in Figure 9a. Note that clouds reaching tops < 7 km do not precipitate.

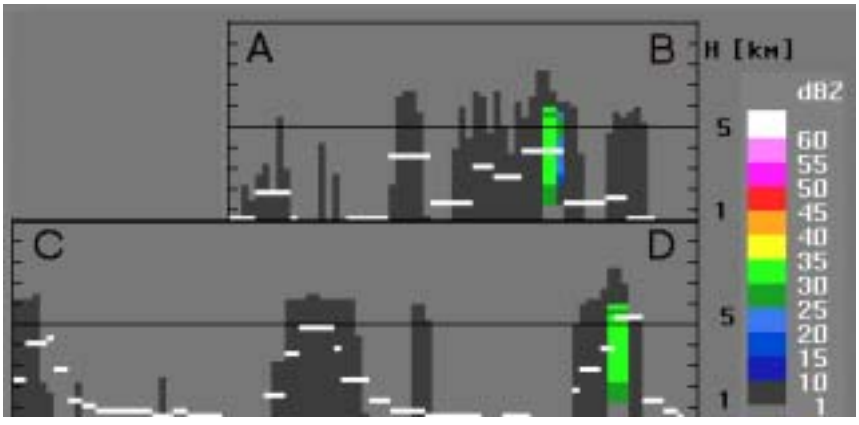

Fig. 10a: A TRMM image showing microphysically continental cumulus and cumulonimbus clouds growing in smoke over the Amazon, centered at 13°S, 61°W, on 18:16 GMT, September 15, 1998. The color scheme is given in Table 1.

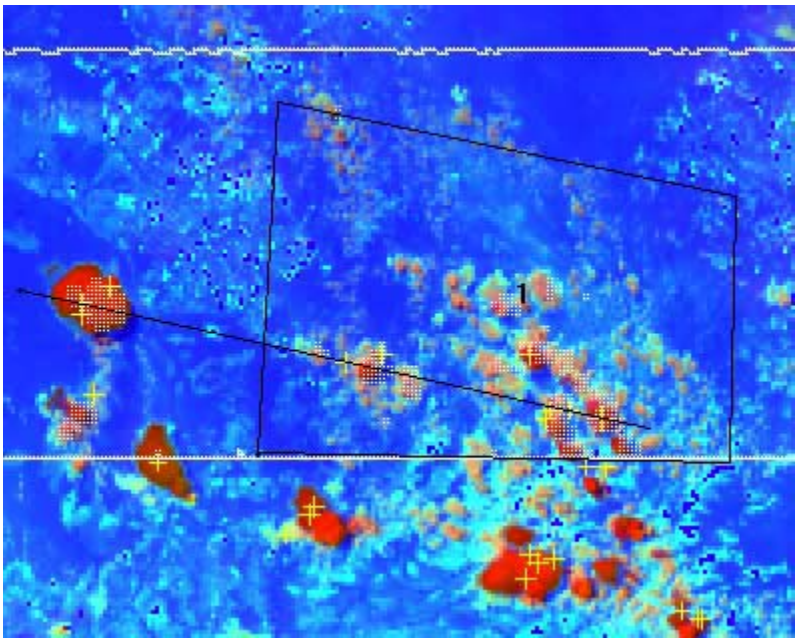

LBXD9809151816_tre_a

Fig. 10b: The T-r_e for the frame in Figure 10a. The lines of the 15th, 50th and 85th percentiles of pixels with re for a given T are plotted. The microphysical zones are marked by the vertical bars where 1 = diffusional growth, 4 = mixed phase and 5 = glaciated. Note that glaciation is indicated at –27°C.

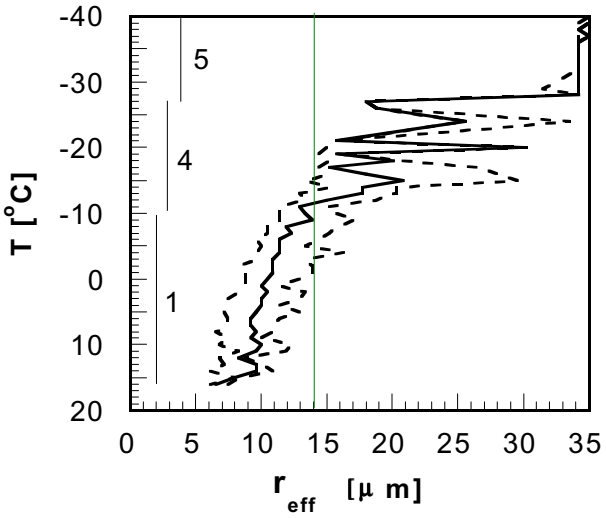

Fig. 10c: The vertical cross section of the clouds along the line in Fig. 10a. Note that that the Z>40 dBZ extends to H=10 km, i.e., well above the 0°C isotherm.

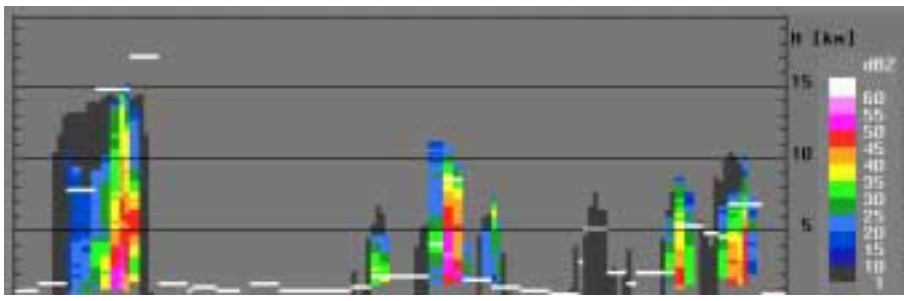

Fig. 11a: A TRMM image showing microphysically maritime cumulus and cumulonimbus clouds growing in clean air over the Amazon, centered at 5°S, 59°W, on 16:28 GMT on April 13, 1998. The color scheme is given in Table 2.

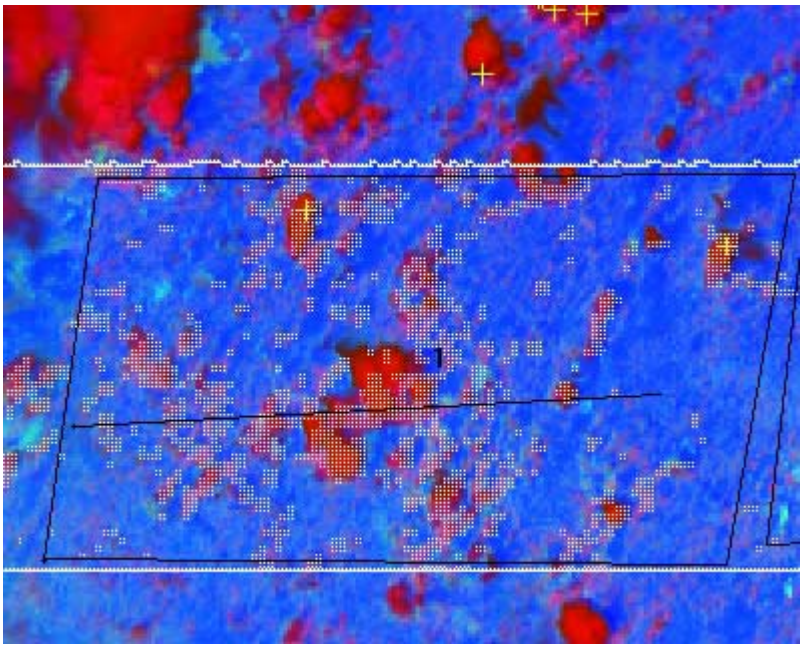

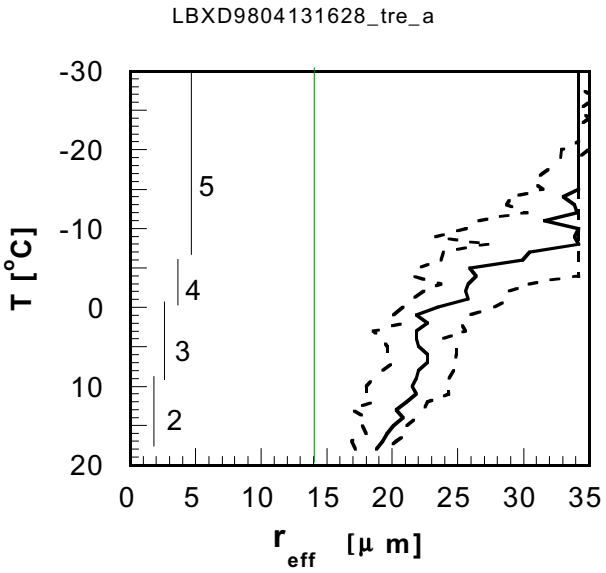

Fig. 11b: The T-r_e plot for the frame in Figure 11a. The microphysical zones are marked by the vertical bars 2 = coalescence, 3 = fallout, 4 = mixed phase and 5 = glaciated zones. Note the deep rainout zone and the glaciation indicated at the relatively high T=-7°C.

.

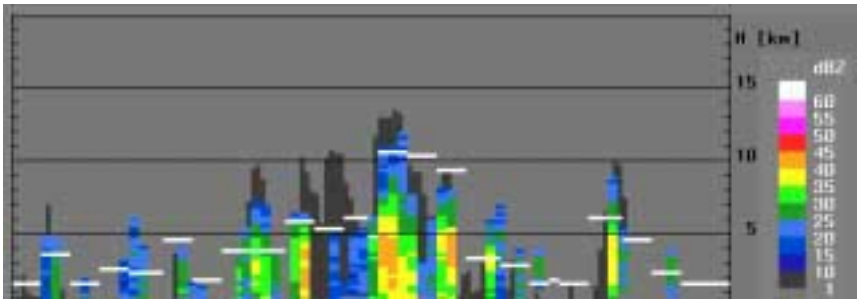

Fig. 11c: The vertical cross section of the clouds along the line in Fig. 9a. Note that the shallowest clouds already precipitate. Also note that the Z>40 dBZ is confined to H<5 km, i.e., below the 0°C isotherm.

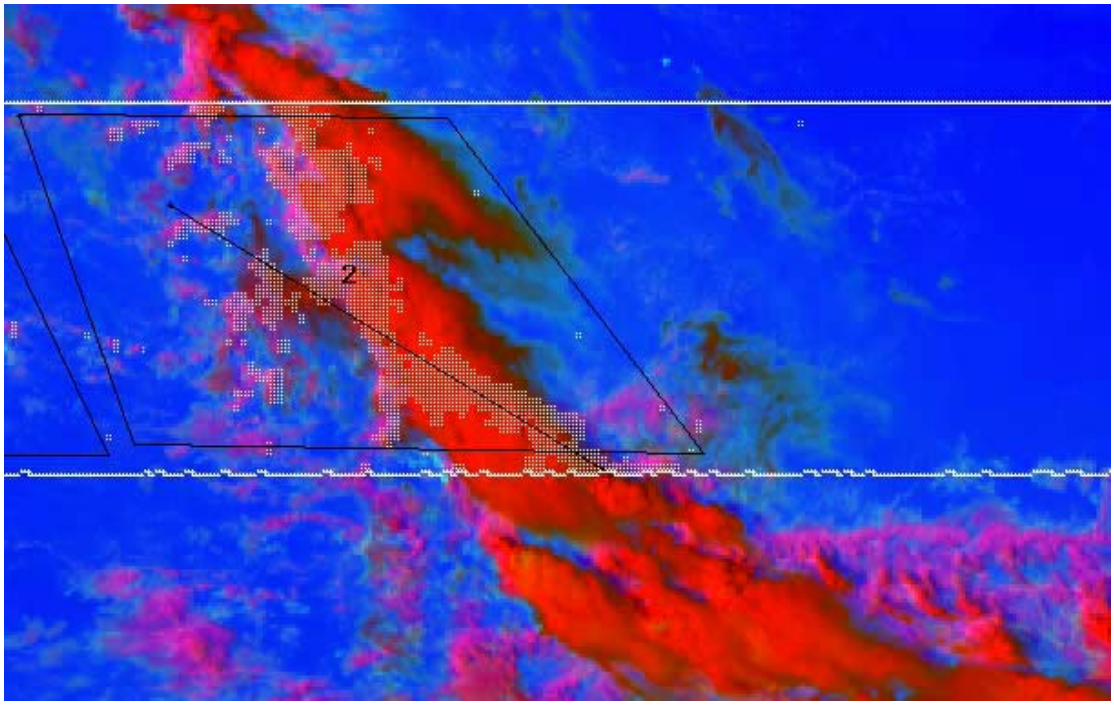

Fig. 12a: A TRMM image showing microphysically maritime cumulus and cumulonimbus clouds over the equatorial Pacific near Kwajalein, centered at 6N 167W, on 02:51 GMT November 5, 1998. The color scheme is given in Table 2.

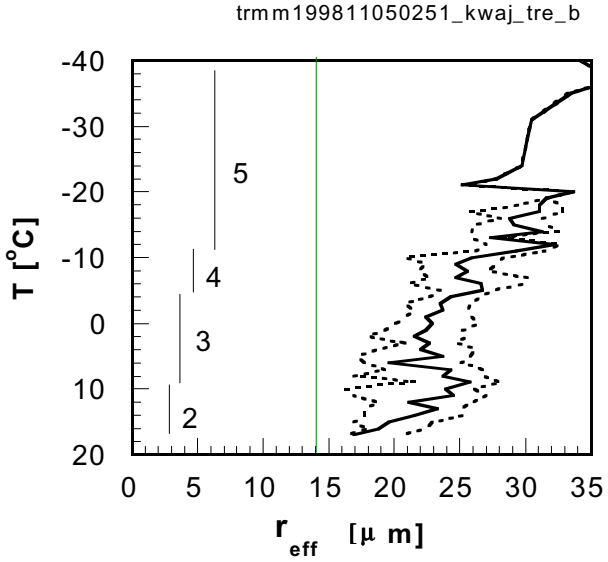

Fig. 12b: The T-r_e for the frame in Figure 12a. Note the great similarity of the microphysical zones to the clouds over the Amazon in the clean air, as shown in Figure 11b.

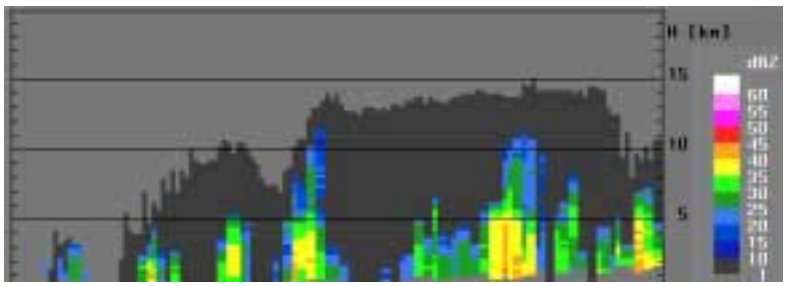

Fig. 12c: The vertical cross section of the clouds along the line in Fig. 12a. Note that the shallowest clouds already precipitate. Also note that the Z>40 dBZ is confined to H<5 km, i.e., below the 0°C isotherm..

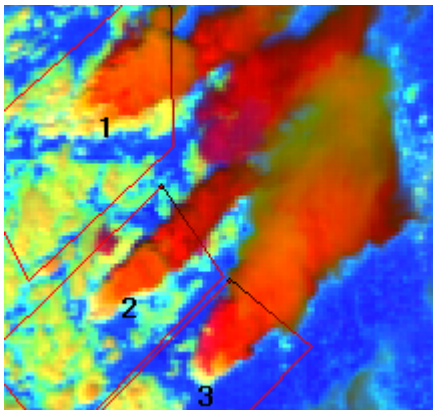

Fig. 13a**:** Hailstorm Cb clouds in an area of about 150x150 km over Alberta, Canada, as observed by the NOAA/AVHRR overpass of 10 July 1998 at 22:15 GMT. According to the color classification scheme presented in Table 2, the yellow cumuliform cloud elements indicate they are composed of supercooled droplets. The red areas are the anvils of the Cb tops.

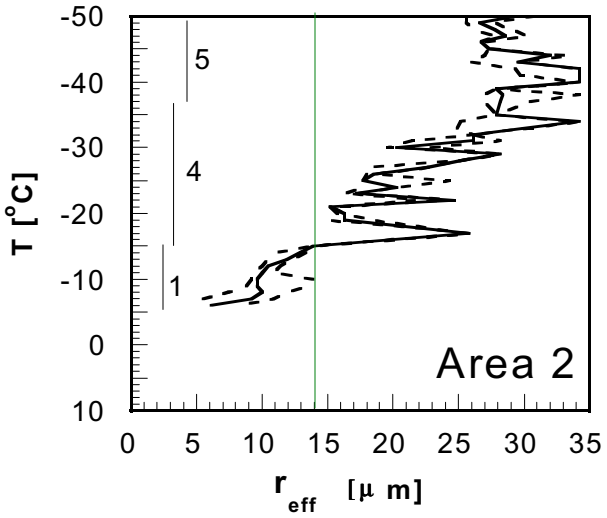

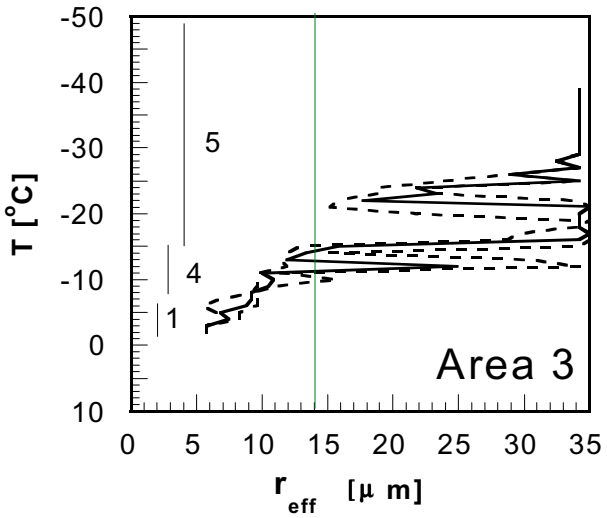

Fig. 13b: The T-r_e for frames 2 and 3 of Fig. 13a. The T- r_e graphs for area #2 shows very deep supercooled water and mixed phase clouds with glaciation occurring only at –37°C. The same applies to Area 1 (not shown). The clouds in Area 3 were seeded with A_gI ice nuclei, and glaciated between –15 to –25°C in different parts of the cloud, as indicated by the T- r_e graph for that area. Hail was observed in the area on that day. However, clouds 1 and 2 occurred over remote areas where there were no observations.

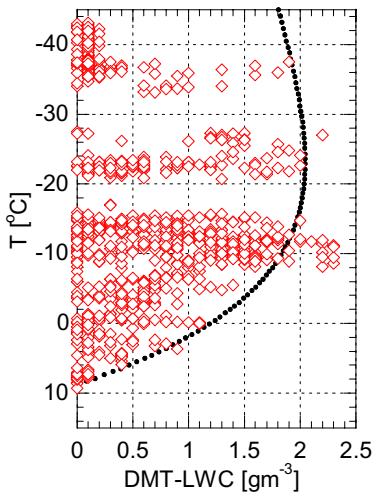

Figure 14a

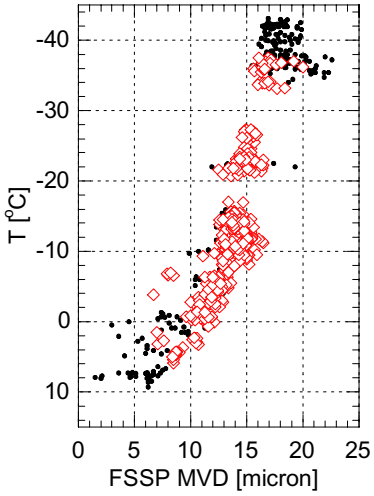

Figure 14b

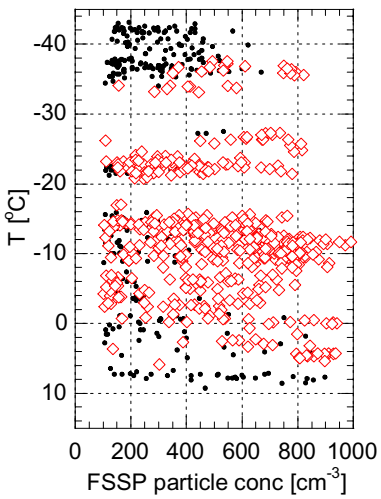

Figure 14c

Fig. 14a: The supercooled cloud liquid water content as a function of temperature, in all the clouds on the 13 August 1999. Each point represents one second of measurements, or 150 - 200 m of cloud path. Note the abrupt decrease of the water at –38°C, indicating the point of homogeneous freezing. The dotted curve marks the ½ adiabatic water content, as a reference for the rate of consumption of cloud water to freezing and other processes. The black dots are those in which the hot wire sensor detected less than 0.3 g m^{-3} liquid water contents.

Fig. 14b: The median volume diameter of the cloud particles measured by a Forward Scattering Spectrometer Probe (FSSP) as a function of temperature, in all the clouds on the 13 August 1999. Each point represents one second of data, or 150 - 200 m of cloud path, containing more than 100 cm^{-3} FSSP-measured cloud particles. The red symbols denote cloud segments with hot-wire measured liquid water contents $\geq$0.3 gm^{-3}.

Fig. 14c: The same as Fig. 2, but for the FSSP-100 measured concentration of cloud particles.

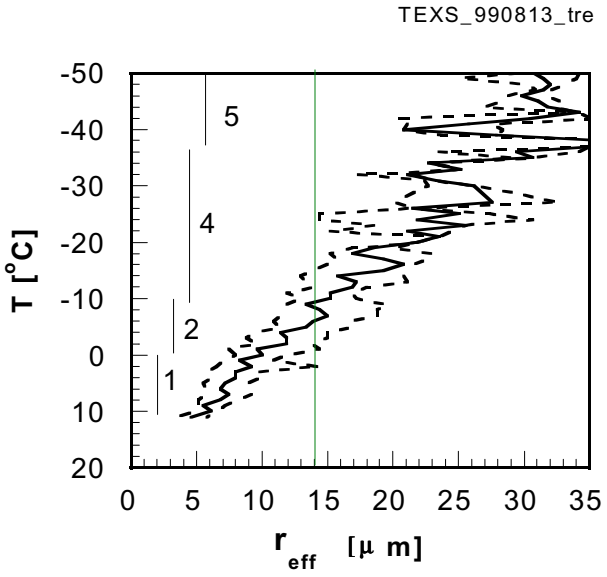

Fig. 15. The T-r_e plots for the TRMM satellite overpass at 22:45 GMT (1745 CDT) on 13 August 1999. The clouds profiled were those in which the aircraft measurements were made. Note that the r_e increased steadily with decreasing T until about –38°C, indicating that only at that temperature were the clouds mostly glaciated.

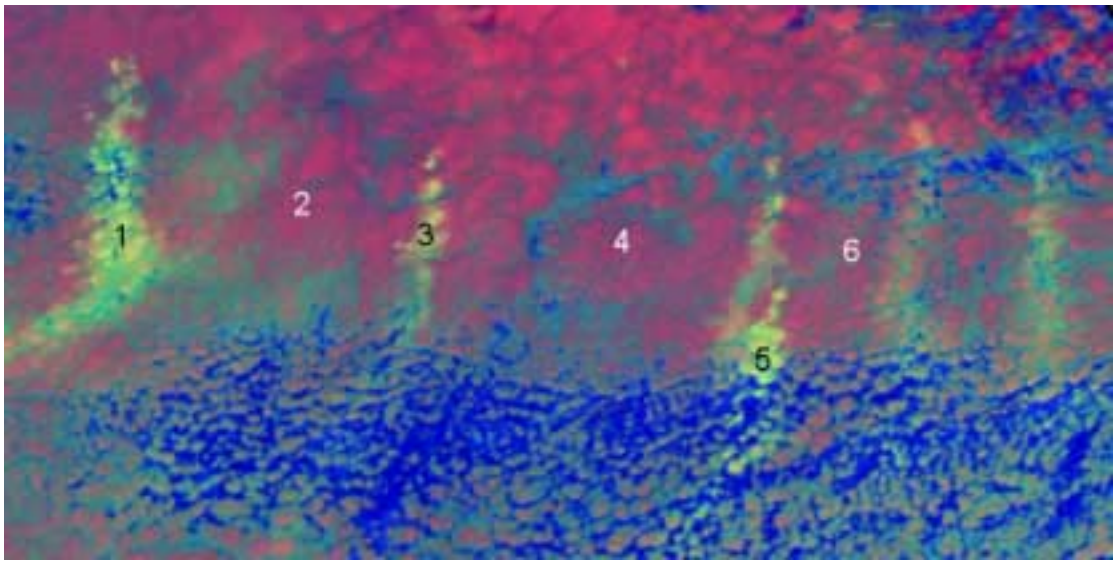

Fig. 16: Processed AVHRR image at 2012 GMT on 20 July 2000 showing five pollution tracks in a supercooled cloud deck in north-central Manitoba Province, Canada. The dimensions of the image is 550X250 km.

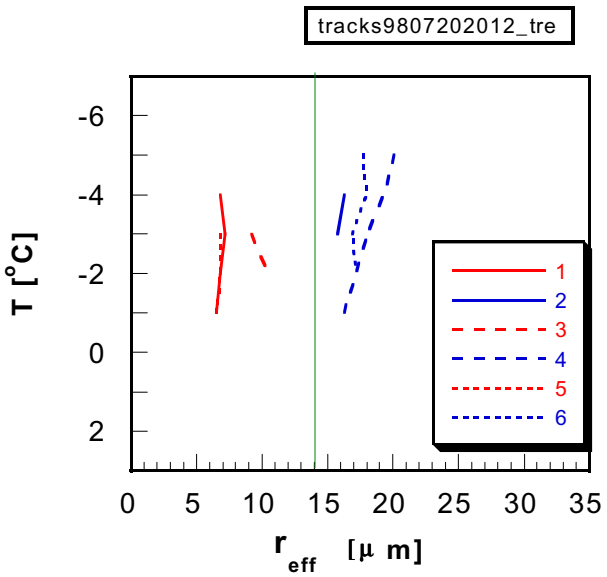

Fig. 17: The effective radius in and outside of the pollution tracks shown in Fig. 16. The numbers in the figure correspond to the numbered areas in Fig. 16.

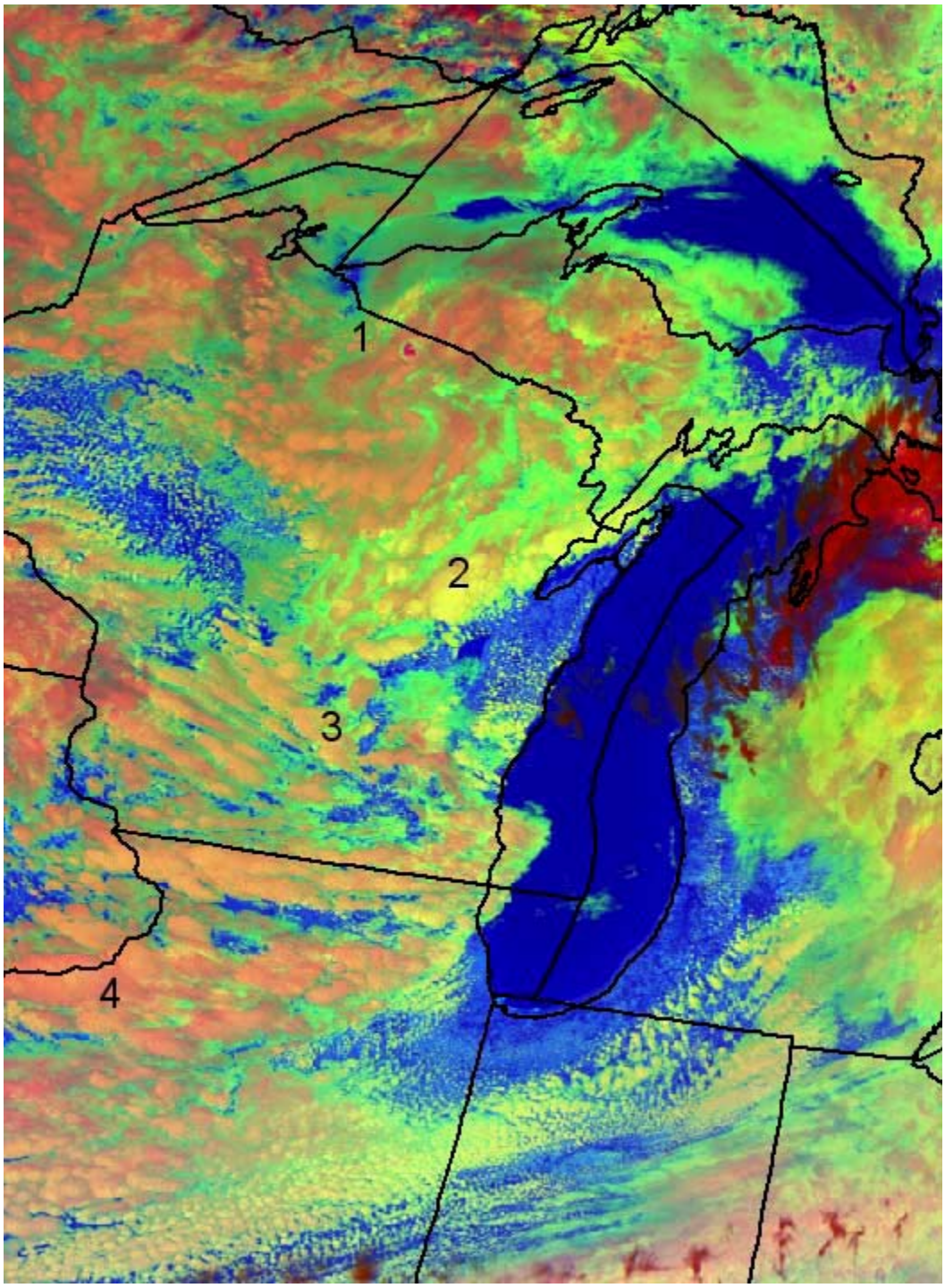

Fig. 18: The AVHRR image for the Great Lakes industrial area at 2007 GMT on 5 June 1998.

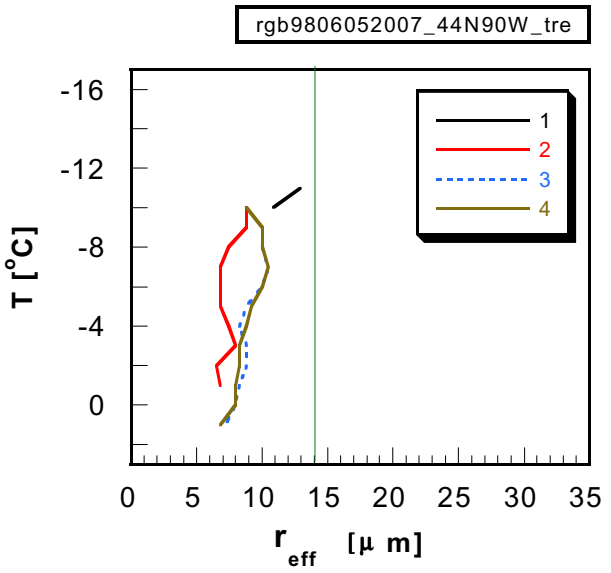

Fig. 19: The T-R_e plots for the four areas shown in Fig. 18. Note that R_e averages 6 to 10 microns between +2°C and –10°C.

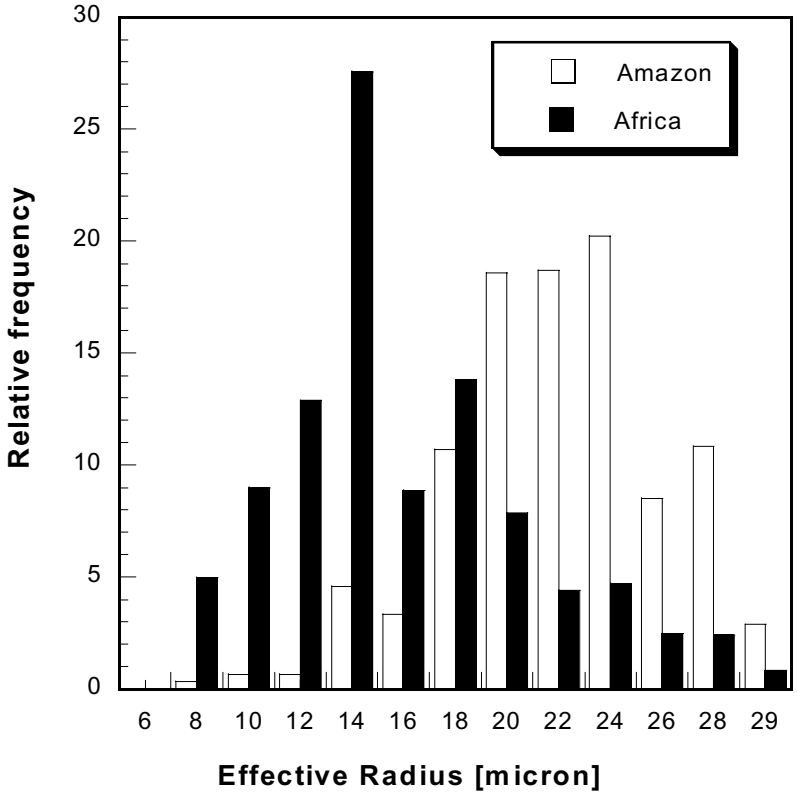

Fig. 20: Plot of the relative frequency of effective cloud radius for clouds over the African Congo (black bars) and the Amazon (crosshatched bars). The plot is excerpted from the paper by McCollum et al. (1999).